Research Department

Technical Report No. 72

Implementation of the Semi-Lagrangian Method in a High Resolution Version of the ECMWF Forecast Model

Harold Ritchie[1],
Clive Temperton, Adrian Simmons, Mariano Hortal,
Terry Davies[2], David Dent and Mats Hamrud

[1] Visiting Scientist at ECMWF, September 1988 - December 1989.
Recherche en prévision numérique,
Atmospheric Environment Service, Dorval, Québec, Canada H9P 1J3

[2] Present address: Meteorological Office, Bracknell, Berkshire RG12 8SZ, U.K.

March 1994, Revised June 1994. Submitted to Monthly Weather Review

Abstract

In this article we examine the implementation of the semi-Lagrangian method in a high resolution version of the ECMWF forecast model. Novel aspects include the application of the semi-Lagrangian scheme to a global model using the ECMWF hybrid coordinate in the vertical, and its use in a baroclinic spectral model in conjunction with a reduced Gaussian grid in the horizontal. The former Eulerian vorticity-divergence formulation is first converted into a momentum-equation formulation which is considerably more economical, thanks in part to the incorporation of Legendre transform efficiencies that were previously demonstrated for the shallow-water equations. The semi-Lagrangian formulation is presented in detail, together with a discussion of computational aspects that are relevant for executing the high resolution model efficiently on a modestly parallel supercomputer. The impact of formulation changes is assessed via numerical experiments on a set of 12 independent cases. In particular it is shown that, by virtue of using a larger timestep, the semi-Lagrangian version is several times more efficient than the Eulerian scheme; that the hybrid-coordinate configuration maintains its design advantage over the sigma-coordinate version in the stratosphere; that the "vertically non-interpolating" scheme performs better than the "fully interpolating" method; and that the increase in horizontal resolution from T106 to T213 (enabled in part by the gains in model efficiency) has a significant positive impact.

CONTENTS

1. Introduction

Since the original demonstration of the efficiency advantage of the semi-Lagrangian semi-implicit method over a decade ago by André Robert, this numerical integration scheme is being used in an increasing range of atmospheric models. Most of the applications have been in gridpoint models. Shallow water equations studies have included three time-level versions by Robert (1981, 1982) and Staniforth and Temperton (1986), and two time-level schemes by Temperton and Staniforth (1987), Purser and Leslie (1988), McDonald and Bates (1989), and Côté and Staniforth (1990). There also have been various applications in baroclinic gridpoint models. Three time-level sigma- coordinate versions have been presented by Robert et al. (1985) and Tanguay et al. (1989), and the extension of the three time-level approach to a non-hydrostatic coordinate has been demonstrated by Tanguay et al. (1990) . Bates and McDonald (1982), McDonald (1986), Leslie and Purser (1991), McDonald and Haugen (1992), and Bates et al. (1993) have developed two time-level sigma-coordinate schemes, McDonald and Haugen (1993) have presented the two time-level extension to a hybrid vertical coordinate, and Golding (1992) has applied a split two time-level semi-Lagrangian scheme in a non-hydrostatic model.

For spectral models, a semi-Lagrangian semi-implicit shallow water equations model was presented by Ritchie (1988) for a three time-level version, and adapted by Côté and Staniforth (1988) for a two time-level scheme. Baroclinic three time-level spectral model formulations have been demonstrated by Ritchie (1991) for operational numerical weather prediction in a sigma-coordinate model, and recently by Williamson and Olson (1994) for climate simulations with a hybrid coordinate model.

In a broader context, the semi-Lagrangian scheme as incorporated in spectral numerical weather prediction models may be considered as an economical variant of the spectral Lagrange-Galerkin method (Süli and Ware, 1991).

Experience at ECMWF (Simmons et al., 1989) suggested that the accuracy of medium-range forecasts had steadily improved with increases in resolution. Consequently, in its four-year plan for the period 1989-1992, ECMWF proposed development of a high-resolution version of its forecast model. A target resolution of a spectral representation with a triangular truncation of 213 waves in the horizontal and 31 levels in the vertical (T213/L31) was set, entailing a doubling of the horizontal resolution and an approximate doubling of the vertical resolution in the troposphere compared to the T106/L19 configuration that was operational at the time (Simmons et al., 1989). In view of the anticipated computer resources, it was clear that major efficiency gains would be necessary in order to attain this objective. These gains have been provided by the introduction of the semi-Lagrangian treatment of advection permitting a substantial increase in the size of the timestep, the use of a reduced Gaussian grid giving a further advantage of about 25%, the introduction of economies in the Legendre transforms, and improvements to the model's basic architecture.

The layout for the remainder of the paper is as follows. In section 2 we present the reformulation of the Eulerian model in order to transform the vorticity-divergence formulation into a momentum-equation version in preparation for a subsequent semi-Lagrangian vector treatment of the equations of motion. The vertical discretization of the ECMWF hybrid coordinate on a staggered grid is also considered. The semi-Lagrangian treatment is discussed in some detail in section 3, including the adaptation to accommodate the reduced Gaussian grid. Section 4 deals with several important computational details that are relevant for efficient execution of the high resolution model on a modestly parallel supercomputer. A series of numerical experiments performed in order to assess the impact of formulation and numerical parameter changes is presented in section 5, followed by a concluding discussion in section 6.

2. Eulerian reformulation

Following Ritchie (1988,1991), the first step in developing a semi-Lagrangian version of the ECMWF spectral model was to convert the existing Eulerian ζ-D (vorticity-divergence) model to a U-V formulation, where U and V are the wind images defined by $U=u\cos\theta$, $V=v\cos\theta$ (u and v are the components of the horizontal wind in spherical coordinates, and θ is latitude). In this section we describe the Eulerian U-V model.

(a) Continuous equations

First we set out the continuous equations in (λ,θ,η) coordinates, where λ is longitude and η is the hybrid vertical coordinate introduced by Simmons and Burridge (1981); thus $\eta\,(p,p_s)$ is a monotonic function of the pressure p, and also depends on the surface pressure p_s in such a way that

$$\eta\,(0,p_s)=0 \text{ and } \eta\,(p_s,p_s)=1.$$

The momentum equations are

$$\frac{\partial U}{\partial t}+\frac{1}{a\cos^2\theta}\left\{U\frac{\partial U}{\partial\lambda}+V\cos\theta\frac{\partial U}{\partial\theta}\right\}+\dot{\eta}\frac{\partial U}{\partial\eta}$$

$$-fV+\frac{1}{a}\left\{\frac{\partial\phi}{\partial\lambda}+R_dT_v\frac{\partial}{\partial\lambda}(\ln p)\right\}=P_U+K_U, \tag{2.1}$$

$$\frac{\partial V}{\partial t}+\frac{1}{a\cos^2\theta}\left\{U\frac{\partial V}{\partial\lambda}+V\cos\theta\frac{\partial V}{\partial\theta}+\sin\theta\,(U^2+V^2)\right\}+\dot{\eta}\frac{\partial V}{\partial\eta}$$

$$+fU+\frac{\cos\theta}{a}\left\{\frac{\partial\phi}{\partial\theta}+R_dT_v\frac{\partial}{\partial\theta}(\ln p)\right\}=P_V+K_V \tag{2.2}$$

where a is the radius of the earth, $\dot{\eta}$ is the η-coordinate vertical velocity ($\dot{\eta}=d\eta/dt$), ϕ is geopotential, R_d is the gas constant for dry air, and T_v is the virtual temperature defined

by

$$T_v = T(1+\{R_v/R_d-1\}q)$$

where T is temperature, q is specific humidity and R_v is the gas constant for water vapour. P_U and P_V represent the contributions of the parameterized physical processes, while K_U and K_V are the horizontal diffusion terms.

The thermodynamic equation is

$$\frac{\partial T}{\partial t} + \frac{1}{a\cos^2\theta}\left\{U\frac{\partial T}{\partial \lambda} + V\cos\theta\frac{\partial T}{\partial \theta}\right\} + \dot{\eta}\frac{\partial T}{\partial \eta} - \frac{\kappa T_v \omega}{(1+(\delta-1)q)p} = P_T + K_T \qquad (2.3)$$

where $\kappa = R_d/C_{pd}$ (C_{pd} is the specific heat of dry air at constant pressure), ω is the p-coordinate vertical velocity ($\omega = dp/dt$), and $\delta = C_{pv}/C_{pd}$ (C_{pv} is the specific heat of water vapour at constant pressure).

The moisture equation is

$$\frac{\partial q}{\partial t} + \frac{1}{a\cos^2\theta}\left\{U\frac{\partial q}{\partial \lambda} + V\cos\theta\frac{\partial q}{\partial \theta}\right\} + \dot{\eta}\frac{\partial q}{\partial \eta} = P_q + K_q \,. \qquad (2.4)$$

In (2.3) and (2.4), P_T and P_q represent the contributions of the parameterized physical processes, while K_T and K_q are the horizontal diffusion terms.

The continuity equation is

$$\frac{\partial}{\partial t}\left(\frac{\partial p}{\partial \eta}\right) + \nabla.\left(\underset{\sim}{V}_H\frac{\partial p}{\partial \eta}\right) + \frac{\partial}{\partial \eta}\left(\dot{\eta}\frac{\partial p}{\partial \eta}\right) = 0 \qquad (2.5)$$

where ∇ is the horizontal gradient operator in spherical coordinates and $\underset{\sim}{V}_H = (u, v)$ is the horizontal wind.

The geopotential ϕ which appears in (2.1) and (2.2) is defined by the hydrostatic equation:

$$\frac{\partial \phi}{\partial \eta} = -\frac{R_d T_v}{p}\frac{\partial p}{\partial \eta} \tag{2.6}$$

while the vertical velocity ω in (2.3) is given by

$$\omega = -\int_0^{\eta} \nabla.\left(\underset{\sim}{V}_H \frac{\partial p}{\partial \eta}\right) d\eta + \underset{\sim}{V}_H.\nabla p \,. \tag{2.7}$$

Expressions for the rate of change of surface pressure, and for the vertical velocity $\dot{\eta}$, are obtained by integrating (2.5), using the boundary conditions $\dot{\eta}=0$ at $\eta=0$ and at $\eta=1$:

$$\frac{\partial p_s}{\partial t} = -\int_0^{1} \nabla.\left(\underset{\sim}{V}_H \frac{\partial p}{\partial \eta}\right) d\eta, \tag{2.8}$$

$$\dot{\eta}\frac{\partial p}{\partial \eta} = -\frac{\partial p}{\partial t} - \int_0^{\eta} \nabla.\left(\underset{\sim}{V}_H \frac{\partial p}{\partial \eta}\right) d\eta \,. \tag{2.9}$$

Since we use $\ln(p_s)$ rather than p_s as the surface pressure variable, it is convenient to rewrite (2.8) as

$$\frac{\partial}{\partial t}(\ln p_s) = -\frac{1}{p_s}\int_0^{1} \nabla.\left(\underset{\sim}{V}_H \frac{\partial p}{\partial \eta}\right) d\eta \,. \tag{2.10}$$

(b) Vertical discretization

To represent the vertical variation of the dependent variables U, V, T and q, the atmosphere is divided into NLEV layers as illustrated in Fig. 1. These layers are defined by the pressures at the interfaces between them (the "half-levels"), and these pressures are given by

$$p_{k+\frac{1}{2}} = A_{k+\frac{1}{2}} + B_{k+\frac{1}{2}} p_s \tag{2.11}$$

for $0 \le k \le NLEV$. The $A_{k+\frac{1}{2}}$ and $B_{k+\frac{1}{2}}$ are constants whose values effectively define the

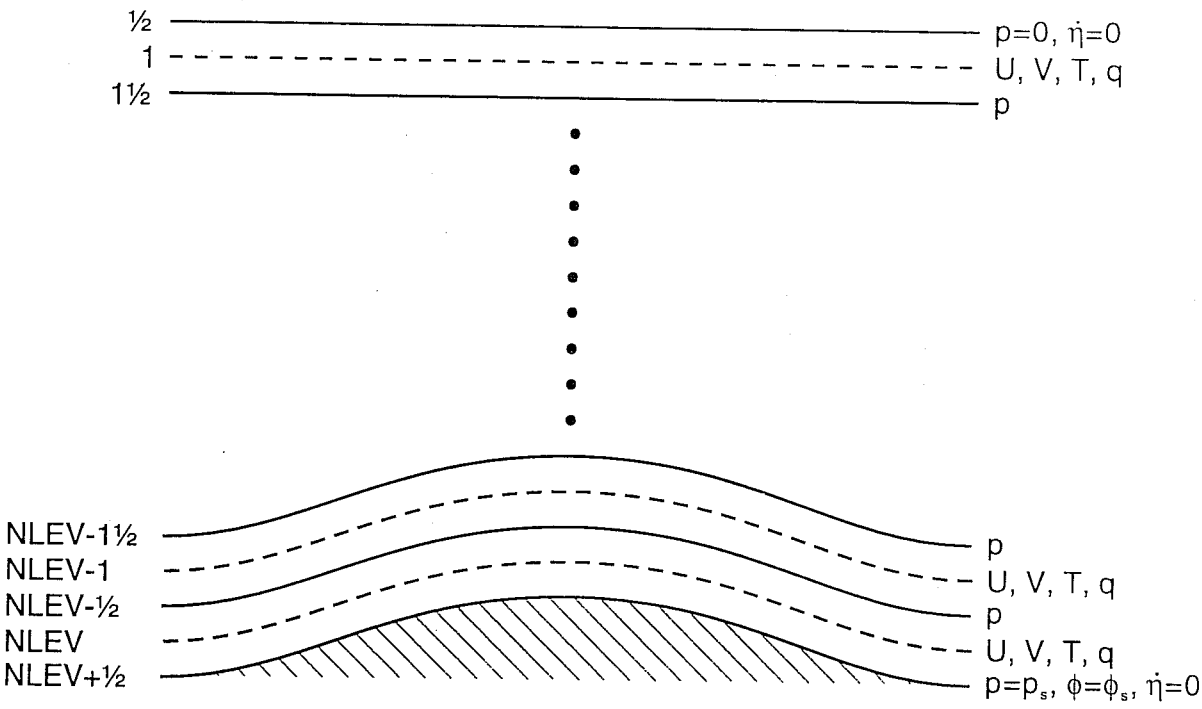

Fig. 1 Vertical distribution of variables.

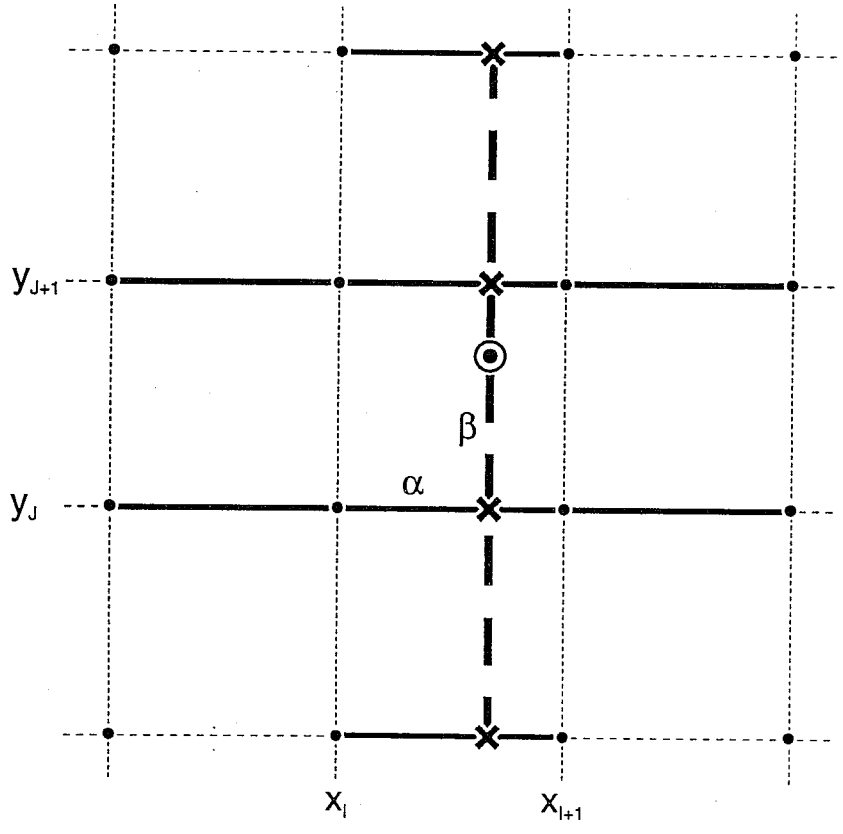

Fig. 2 Schematic diagram illustrating "quasi-cubic" interpolation.

vertical coordinate.

The prognostic variables are represented by their values at "full-level" pressures p_k. Values for p_k are not explicitly required by the model's vertical finite-difference scheme, which is described below.

The discrete analogue of the surface pressure tendency equation (2.10) is

$$\frac{\partial}{\partial t}(\ln p_s) = -\frac{1}{p_s}\sum_{k=1}^{NLEV} \nabla.(\underset{\sim}{V}_k \Delta p_k) \tag{2.12}$$

where

$$\Delta p_k = p_{k+½} - p_{k-½} . \tag{2.13}$$

From (2.11) we obtain

$$\frac{\partial}{\partial t}(\ln p_s) = -\sum_{k=1}^{NLEV} \{\frac{1}{p_s} D_k \Delta p_k + (\underset{\sim}{V}_k . \nabla \ln p_s) \Delta B_k\} \tag{2.14}$$

where D_k is the divergence at level k,

$$D_k = \frac{1}{a\cos^2\theta}\left(\frac{\partial U_k}{\partial \lambda} + \cos\theta \frac{\partial V_k}{\partial \theta}\right) \tag{2.15}$$

and

$$\Delta B_k = B_{k+½} - B_{k-½} . \tag{2.16}$$

The discrete analogue of (2.9) is

$$\left(\dot{\eta}\frac{\partial p}{\partial \eta}\right)_{k+½} = -\frac{\partial p_{k+½}}{\partial t} - \sum_{j=1}^{k} \nabla.(\underset{\sim}{V}_j \Delta p_j) \tag{2.17}$$

and from (2.11) we obtain

$$\left(\dot{\eta}\frac{\partial p}{\partial \eta}\right)_{k+½} = -p_s\left[B_{k+½}\frac{\partial}{\partial t}(\ln p_s) + \sum_{j=1}^{k} \{\frac{1}{p_s} D_j \Delta p_j + (\underset{\sim}{V}_j . \nabla \ln p_s)\Delta B_j\}\right] \tag{2.18}$$

where $\frac{\partial}{\partial t}(\ln p_s)$ is given by (2.14).

Vertical advection of a variable X is now given by

$$\left(\dot{\eta}\frac{\partial X}{\partial \eta}\right)_k = \frac{1}{2\Delta p_k}\left\{\left(\dot{\eta}\frac{\partial p}{\partial \eta}\right)_{k+\frac{1}{2}}(X_{k+1}-X_k) + \left(\dot{\eta}\frac{\partial p}{\partial \eta}\right)_{k-\frac{1}{2}}(X_k-X_{k-1})\right\}. \tag{2.19}$$

The discrete analogue of the hydrostatic equation (2.6) is

$$\phi_{k+\frac{1}{2}} - \phi_{k-\frac{1}{2}} = -R_d(T_v)_k \ln\frac{p_{k+\frac{1}{2}}}{p_{k-\frac{1}{2}}} \tag{2.20}$$

which gives

$$\phi_{k+\frac{1}{2}} = \phi_s + \sum_{j=k+1}^{NLEV} R_d(T_v)_j \ln\frac{p_{j+\frac{1}{2}}}{p_{j-\frac{1}{2}}} \tag{2.21}$$

where ϕ_s is the geopotential at the surface. Full-level values of the geopotential, as required in the momentum equations (2.1) and (2.2), are given by

$$\phi_k = \phi_{k+\frac{1}{2}} + \alpha_k R_d(T_v)_k \tag{2.22}$$

where $\alpha_1 = \ln 2$ and, for $k>1$,

$$\alpha_k = 1 - \frac{p_{k-\frac{1}{2}}}{\Delta p_k}\ln\left(\frac{p_{k+\frac{1}{2}}}{p_{k-\frac{1}{2}}}\right). \tag{2.23}$$

The remaining part of the pressure gradient terms in (2.1) and (2.2) is given by

$$R_d(T_v\nabla \ln p)_k = \frac{R_d(T_v)_k}{\Delta p_k}\left\{\left(\ln\frac{p_{k+\frac{1}{2}}}{p_{k-\frac{1}{2}}}\right)\nabla p_{k-\frac{1}{2}} + \alpha_k\nabla(\Delta p_k)\right\} \tag{2.24}$$

with α_k given by (2.23) for all k.

Finally, the energy conversion term in the thermodynamic equation (2.3) is discretized as

$$\frac{\kappa T_v \omega}{(1+(\delta-1)q)p}$$

$$= \frac{\kappa (T_v)_k}{1+(\delta-1)q_k}\left\{-\frac{1}{\Delta p_k}\left\{(\ln\frac{p_{k+\frac{1}{2}}}{p_{k-\frac{1}{2}}})\sum_{j=1}^{k-1}(D_j\Delta p_j + p_s(\underset{\sim}{v}_j.\nabla \ln p_s)\Delta B_j)\right.\right.$$

$$\left. + \alpha_k(D_k\Delta p_k + p_s(\underset{\sim}{v}_k.\nabla \ln p_s)\Delta B_k)\right\}$$

$$\left. + \frac{p_s}{\Delta p_k}\left\{\Delta B_k + \frac{C_k}{\Delta p_k}\ln\frac{p_{k+\frac{1}{2}}}{p_{k-\frac{1}{2}}}\right\}(\underset{\sim}{v}_k.\nabla \ln p_s)\right\} \qquad (2.25)$$

where $\alpha_1 = \ln 2$, α_k is defined by (2.23) for $k>1$, and

$$C_k = A_{k+\frac{1}{2}}B_{k-\frac{1}{2}} - A_{k-\frac{1}{2}}B_{k+\frac{1}{2}} . \qquad (2.26)$$

The reasons behind the various choices made in this vertical discretization scheme are discussed by Simmons and Burridge (1981); basically the scheme is designed to conserve angular momentum and energy for frictionless adiabatic flow.

(c) Time discretization

To introduce a discretization in time, together with a semi-implicit correction, we define the operators

$$\delta_t X = (X^+ - X^-)/2\Delta t ,$$

$$\Delta_{tt} X = (X^+ - 2X + X^-) ,$$

where X represents the value of a variable at time t, X^+ the value at time $(t+\Delta t)$, and X^- the value at $(t-\Delta t)$. In preparation for the semi-Lagrangian treatment to be developed in Section 3, we also introduce the three-dimensional advection operator

$$A(X) = \frac{1}{a\cos^2\theta}\left(U\frac{\partial X}{\partial \lambda} + V\cos\theta\frac{\partial X}{\partial \theta}\right) + \dot{\eta}\frac{\partial X}{\partial \eta} . \qquad (2.27)$$

Introducing the semi-implicit correction terms, Equations (2.1)-(2.4) become:

$$\delta_t U + A(U) - fV + \frac{1}{a}\left\{\frac{\partial \phi}{\partial \lambda} + R_d T_v \frac{\partial}{\partial \lambda}(\ln p)\right\}$$

$$= P_U + K_U - \frac{\beta}{2a}\Delta_{tt}\left\{\underline{\underline{\gamma}}\frac{\partial T}{\partial \lambda} + R_d T_r \frac{\partial}{\partial \lambda}(\ln p_s)\right\} \tag{2.28}$$

$$\delta_t V + A(V) + \frac{\sin\theta}{a\cos^2\theta}(U^2+V^2) + fU + \frac{\cos\theta}{a}\left\{\frac{\partial \phi}{\partial \theta} + R_d T_v \frac{\partial}{\partial \theta}(\ln p)\right\}$$

$$= P_V + K_V - \frac{\beta\cos\theta}{2a}\Delta_{tt}\left\{\underline{\underline{\gamma}}\frac{\partial T}{\partial \theta} + R_d T_r \frac{\partial}{\partial \theta}(\ln p_s)\right\} \tag{2.29}$$

$$\delta_t T + A(T) - \frac{\kappa T_v \omega}{(1+(\delta-1)q)p} = P_T + K_T - \frac{\beta}{2}\Delta_{tt}(\underline{\underline{\tau}}D) \tag{2.30}$$

$$\delta_t q + A(q) = P_q + K_q \tag{2.31}$$

where β is a parameter of the semi-implicit scheme; the classical scheme (Robert 1969) is recovered with $\beta=1$. The semi-implicit correction terms are linearized versions of the pressure gradient terms in (2.1)-(2.2) and the energy conversion term in (2.3). Thus T_r is a reference temperature (here chosen to be independent of vertical level), while $\underline{\underline{\gamma}}$ and $\underline{\underline{\tau}}$ are matrices such that

$$(\underline{\underline{\gamma}}\underline{\tilde{T}})_k = \alpha_k^r R_d T_k + \sum_{j=k+1}^{NLEV} R_d T_j \ln\left(\frac{p_{j+\frac{1}{2}}^r}{p_{j-\frac{1}{2}}^r}\right) , \tag{2.32}$$

$$(\underline{\underline{\tau}}\underline{\tilde{D}})_k = \kappa T_r\left\{\frac{1}{\Delta p_k^r}\ln\left(\frac{p_{k+\frac{1}{2}}^r}{p_{k-\frac{1}{2}}^r}\right)\sum_{j=1}^{k-1}(D_j \Delta p_j^r) + \alpha_k^r D_k\right\} , \tag{2.33}$$

where the half-level pressures appearing in (2.32), (2.33) are reference values obtained from (2.11) by choosing a reference value (p_s^r) of p_s, and the coefficients α_k^r are based on these reference values. The reference values adopted for the semi-implicit scheme are T_r=300K and p_s^r=800hPa.

The integrated surface pressure tendency equation (2.14) becomes

$$\delta_t(\ln p_s) + \sum_{k=1}^{NLEV} \left\{ \frac{1}{p_s} D_k \Delta p_k + (\underset{\sim}{v}_k . \nabla \ln p_s) \Delta B_k \right\} = -\frac{\beta}{2} \Delta_{tt}(\underline{\underline{v}} D) \qquad (2.34)$$

where

$$\underline{\underline{v}} D = \frac{1}{p_s^r} \sum_{j=1}^{NLEV} D_j \Delta p_j^r \quad . \qquad (2.35)$$

(d) Horizontal grid

A novel feature of the model is the optional use of a reduced Gaussian grid, as described by Hortal and Simmons (1991). Thus, the number of points on each latitude row is chosen so that the local east-west gridlength remains approximately constant, with the restriction that the number should be suitable for the FFT ($N=2^p 3^q 5^r$). After some experimentation, the "fully reduced grid" option of Hortal and Simmons was implemented; all possible wavenumbers (up to the model's truncation limit) are used in the Legendre transforms. A small amount of noise in the immediate vicinity of the poles was removed by increasing the number of gridpoints in the three most northerly and southerly rows of the grid (from 6, 12 and 18 points in the original design of the T213 grid to 12, 16 and 20 points respectively). Courtier and Naughton (1994) have very recently reconsidered the design of reduced Gaussian grids.

(e) Time-stepping procedure

The time-stepping procedure for the Eulerian U-V version of the model follows closely that outlined by Temperton (1991) for the shallow-water equations. At the start of a timestep, the model state at time $(t-\Delta t)$ is defined by the values of U, V, T, q and $\ln p_s$ on the Gaussian grid. To compute the semi-implicit corrections, the $(t-\Delta t)$ values of

divergence D, $\partial P/\partial\lambda$ and $\partial P/\partial\mu$ are also held on the grid, where $\mu=\sin\theta$ and

$$P = \underline{\gamma}T + R_d T_r \ln p_s \quad . \tag{2.36}$$

The model state at time t is defined by the spectral coefficients of ζ, D, T, q and $\ln p_s$. Legendre transforms followed by Fourier transforms are then used to compute ζ, D, U, V, T, $\partial T/\partial\mu$, q, $\partial q/\partial\mu$, $\ln p_s$ and $\partial(\ln p_s)/\partial\mu$ at time t on the model grid. Additional Fourier transforms are used to compute the corresponding values of $\partial U/\partial\lambda$, $\partial V/\partial\lambda$, $\partial T/\partial\lambda$, $\partial q/\partial\lambda$ and $\partial(\ln p_s)/\partial\lambda$. The meridional gradients of U and V are obtained using the relationships

$$\cos\theta\frac{\partial U}{\partial\theta} = \frac{\partial V}{\partial\lambda} - a\zeta\cos^2\theta \ ,$$

$$\cos\theta\frac{\partial V}{\partial\theta} = aD\cos^2\theta - \frac{\partial U}{\partial\lambda} \quad .$$

All the information is then available to evaluate the terms at time t on the left-hand sides of (2.28)-(2.31) and (2.34), and thus to compute "provisional" tendencies of the model variables. These tendencies (together with values of the variables at $t-\Delta t$) are supplied to the physical parameterization routines, which increment the tendencies with their respective contributions. The semi-implicit correction terms evaluated at time-levels $(t-\Delta t)$ and t are then added to the tendencies. Ignoring the horizontal diffusion terms (which are handled later in spectral space), and grouping together the terms which have been computed on the grid, (2.28)-(2.31) and (2.34) can be written in the form

$$U^+ + \frac{\beta\Delta t}{a}\frac{\partial P^+}{\partial\lambda} = R_1 \tag{2.37}$$

$$V^+ + \frac{\beta\Delta t}{a}\cos\theta\frac{\partial P^+}{\partial\theta} = R_2 \tag{2.38}$$

$$T^+ + \beta\Delta t\underline{\underline{\tau}}D^+ = R_3 \tag{2.39}$$

$$q^+ = R_4 \tag{2.40}$$

$$(\ln p_s)^+ + \beta\Delta t\underline{\underline{\nu}}D^+ = R_5 \ .$$

The right-hand sides R_1–R_5 are transformed to spectral space via Fourier transforms followed by Gaussian integration. The curl and divergence of (2.37) and (2.38) are then computed in spectral space, leading to

$$\zeta^+ = \text{curl}\,(R_1, R_2) \tag{2.42}$$

$$D^+ + \beta\Delta t\nabla^2 P^+ = \text{div}\,(R_1, R_2) \ . \tag{2.43}$$

Equations (2.39), (2.41) and (2.43) can then be combined with the aid of (2.36) to obtain an equation of the form

$$(\underline{\underline{I}} + \frac{n(n+1)}{a^2}\underline{\underline{\Gamma}})\,(D_n^m)^+ = (\tilde{D})_n^m \tag{2.44}$$

for each zonal wavenumber m and total wavenumber n, where the matrix

$$\underline{\underline{\Gamma}} = \beta^2(\Delta t)^2(\underline{\underline{\gamma}}\underline{\underline{\tau}} + R_d T_r \underline{\underline{\nu}}) \tag{2.45}$$

couples all the *NLEV* values of $(D_n^m)^+$ in a vertical column. Once D^+ has been found, the calculation of T^+ and $(\ln p_s)^+$ can be completed, while q^+ and ζ^+ have already been obtained from (2.40) and (2.42).

Finally, a "fractional step" approach is used to implement the horizontal diffusion of vorticity, divergence, temperature and specific humidity. A simple linear diffusion of order $2p$ is applied along the hybrid coordinate surfaces:

$$K_X = -(-1)^p K\nabla^{2p}X \tag{2.46}$$

where $X = \zeta, D$ or q. It is applied in spectral space to the $(t+\Delta t)$ values such that if X_n^m is the spectral coefficient of X prior to diffusion, then the diffused value $\overline{X}_n^m$ is given by

$$\overline{X}_n^m = \{1+2\Delta t K\left(\frac{n(n+1)}{a^2}\right)^p\}^{-1} X_n^m \quad . \tag{2.47}$$

A modified form of (2.47) is also used for the temperature T, to approximate diffusion on surfaces of constant pressure rather than on the sloping hybrid coordinate surfaces (Simmons, 1987). The operational version of the model uses fourth-order horizontal diffusion (p=2).

(f) Time-filtering

To avoid decoupling of the solutions at odd and even timesteps, a Robert filter (Asselin 1972) is applied at each timestep. The time-filtering is defined by

$$X_f = X + \varepsilon (X_f^- - 2X + X^+) \tag{2.48}$$

where the subscript f denotes a filtered value, and X^-, X and X^+ represent values at $(t-\Delta t), t$ and $(t+\Delta t)$ respectively.

Because of the scanning structure of the model (see Section 4), it is convenient to apply the time-filtering in gridpoint space, and to split (2.48) into two parts:

$$\tilde{X}_f = X + \varepsilon (X_f^- - 2X) \tag{2.49}$$

$$X_f = \tilde{X}_f + \varepsilon X^+ \quad . \tag{2.50}$$

The "partially filtered" values computed by (2.49) are stored on a gridpoint work file and passed from one timestep to the next. Thus, the information available after the transforms to gridpoint space consists of partially filtered values at time $(t-\Delta t)$ together with unfiltered values at time t. The filtering of the $(t-\Delta t)$ fields can then be completed via (2.50), which after shifting by one timestep becomes:

$$X_F^- = \tilde{X}_F^- + \varepsilon X \,. \tag{2.51}$$

The computations described in Section 2(e) are performed using these fully filtered values at time $(t-\Delta t)$ and the unfiltered values at time t. Once (2.51) has been implemented, values of X_F^- are also available to implement (2.49) for the partially filtered values to be passed on to the next timestep.

(g) Remarks

Ritchie (1988) noted that for a spectral model of the shallow-water equations, the $U-V$ form and the $\zeta-D$ form gave identical results (apart from round-off error). In extending this work to a multi-level model, Ritchie(1991) found that this equivalence was not maintained. This was in fact a result of some *analytic* manipulations in the vertical, used to eliminate between the variables in solving the equations of the semi-implicit scheme, which were not exactly matched by the finite-element vertical discretization of Ritchie's model.

In the case of the model described here, the corresponding elimination between the variables is purely algebraic, and the equivalence between the $U-V$ form and the $\zeta-D$ form is maintained apart from one small exception due to the use of the hybrid vertical coordinate. In the $U-V$ model, the gradients of the geopotential ϕ are computed in gridpoint space (from the spectrally computed gradients of T, q and $\ln p_s$), while in the $\zeta-D$ model ϕ itself is computed and transformed separately into spectral space, where its Laplacian is added into the divergence equation. Since ϕ is not a quadratic function of the model variables there is some aliasing, which is different for the two versions of the model. In practice the differences between the $\zeta-D$ model and the $U-V$ model were found to be very small, and in the case of a pure sigma-coordinate the two models would be algebraically equivalent.

The $U-V$ model is nevertheless considerably more economical than its $\zeta-D$

counterpart in terms of the number of Legendre transforms required. In addition to the transform of ϕ referred to above, four Legendre transforms are saved in the treatment of the wind fields using the procedures described by Temperton (1991) for the shallow-water equations. The number of multi-level Legendre transforms is thereby reduced from 17 to 12 per timestep.

(h) T_v as spectral variable

In preparation for a further reduction in the number of Legendre transforms required by the semi-Lagrangian version of the model, the modified Eulerian version includes an option to keep the virtual temperature T_v rather than the temperature T as the spectral variable. In the time-stepping procedure, Legendre transforms followed by Fourier transforms are used to compute T_v, $\partial T_v/\partial\mu$ and $\partial T_v/\partial\lambda$ at time t on the model grid; the corresponding vaues of T, $\partial T/\partial\mu$ and $\partial T/\partial\lambda$ are then computed using the corresponding values of q, $\partial q/\partial\mu$ and $\partial q/\partial\lambda$. The thermodynamic equation (2.3) is then stepped forward in time exactly as before. After the physical parameterization routines, the "provisional" value of $T(t+\Delta t)$ is combined with $q(t+\Delta t)$ to compute a provisional value of $T_v(t+\Delta t)$. The semi-implicit correction terms evaluated at time-levels $(t-\Delta t)$ and t are then added to the provisional value of $T_v(t+\Delta t)$, just before the transform back to spectral space.

There are corresponding slight changes in the semi-implicit correction terms. The linearized hydrostatic matrix $\underline{\underline{\gamma}}$ in (2.28)-(2.29) and (2.36) now operates on T_v rather than on T. From the point of view of the semi-implicit scheme, (2.30) has implicitly been replaced by an equation of the form

$$\delta_t T_v = \ldots - \frac{\beta}{2}\Delta_{tt}(\underline{\underline{\tau}}D) \qquad (2.52)$$

although as explained above it is not necessary to formulate or compute the missing terms explicitly. Hence, (2.39) is replaced by

$$T_v^+ + \beta\Delta t\underline{\underline{\tau}}D^+ = R_3' \tag{2.53}$$

and the solution of the semi-implicit equations in spectral space proceeds just as before.

This change of spectral variable results in only insignificant changes to a 10-day model forecast, but permits useful economies in the semi-Lagrangian version to be described in the next section.

3. Semi-Lagrangian formulation

(a) General description

The general form of the model equations is

$$\frac{dX}{dt} \equiv \frac{\partial X}{\partial t} + A(X) = R \tag{3.1}$$

where the three-dimensional advection operator A was defined in (2.27). A three-time-level semi-Lagrangian treatment of (3.1) is obtained by finding the approximate trajectory, over the time interval $[t-\Delta t, t+\Delta t]$, of a particle which arrives at each gridpoint $\underset{\sim}{x}$ at time $(t+\Delta t)$. Equation (3.1) is then approximated by

$$\frac{X^+ - X^-}{2\Delta t} = R^0 \tag{3.2}$$

where the superscripts $+, 0, -$ respectively denote evaluation at the arrival point $(\underset{\sim}{x}, t+\Delta t)$, the mid-point of the trajectory $(\underset{\sim}{x}-\underset{\sim}{\alpha}, t)$, and the departure point $(\underset{\sim}{x}-2\underset{\sim}{\alpha}, t-\Delta t)$. Since the mid-point and the departure point will not in general coincide with model gridpoints, X^- and R^0 must be determined by interpolation.

It is more economical (and, as discussed later, gives better results in some circumstances; see also Tanguay et al., 1992) to evaluate the right-hand side of (3.2) as

$$R^0 = \frac{1}{2}[R(\underset{\sim}{x}-2\underset{\sim}{\alpha}, t) + R(\underset{\sim}{x}, t)] \tag{3.3}$$

since only a single interpolation [of the combined field $X(t-\Delta t)+\Delta t R(t)$ at the point $(\underset{\sim}{x}-2\underset{\sim}{\alpha})$] is then required in order to determine X^+.

The right-hand sides of the time-discretized model equations also contain semi-implicit correction terms, which in the Eulerian model took the form

$$\Delta_{tt} X = (X^+ - 2X^0 + X^-)$$

where the superscripts refer to time-levels, and to a single common gridpoint. In the semi-

Lagrangian version of the model, the semi-implicit correction terms take the form

$$\Delta_{tt}X = (X(\underset{\sim}{x}, t+\Delta t) - X(\underset{\sim}{x}, t)) + (X(\underset{\sim}{x}-2\underset{\sim}{\alpha}, t-\Delta t) - X(\underset{\sim}{x}-2\underset{\sim}{\alpha}, t)) \qquad (3.4)$$

and again the terms to be evaluated at the departure point $(\underset{\sim}{x}-2\underset{\sim}{\alpha})$ can be added to other right-hand side terms before interpolation. Notice that the evaluation of $\Delta_{tt}X$, and both ways of evaluating R^0, are all centered in space and time.

To obtain accurate results from a semi-Lagrangian integration scheme, it is necessary to choose the order of interpolation carefully (see for example Staniforth and Côté, 1991). In practice it has been found (for the model described here) that linear interpolation is adequate for the terms evaluated at the midpoint of the trajectory, but that cubic interpolation is essential for the terms evaluated at the departure point. Cubic interpolation in three dimensions is expensive, and fortunately a "quasi-cubic" interpolation (suggested by Philippe Courtier) was found to give essentially equivalent results. The technique is illustrated in Fig. 2 for two-dimensional interpolation on a regular grid. The target point is at $(x_I+\alpha, y_J+\beta)$. In the first step, four interpolations are performed in the x-direction: *linear* (rather than the usual cubic) interpolations to the points $(x_I+\alpha, y_{J-1})$ and $(x_I+\alpha, y_{J+2})$, and *cubic* interpolations to the points $(x_I+\alpha, y_J)$ and $(x_I+\alpha, y_{J+1})$. In the second step, one cubic interpolation is performed in the y-direction, to evaluate the field at the target point. The number of "neighbours" contributing to the result is reduced from 16 to 12. The generalization to three dimensions is straightforward and results in a significant saving, the number of neighbours being reduced from 64 to 32, and the computation being reduced from 21 one-dimensional cubic interpolations to 7 cubic plus 10 linear one-dimensional interpolations.

For the reduced Gaussian grid described in Section 2(d), the mesh is no longer regular. However, it is easily seen that the extra complication is relatively minor provided that the first step in the interpolation is performed in the λ-direction.

The order of the interpolation in the vertical is reduced to linear when the evaluation point lies between the two highest model levels, or between the lowest two model levels. Extrapolation beyond the top or bottom levels is not allowed.

(b) Finding the departure point

Extending the procedure of Robert (1981) to three dimensions, the midpoint $(\underset{\sim}{x}-\underset{\sim}{\alpha})$ and the departure point $(\underset{\sim}{x}-2\underset{\sim}{\alpha})$ of the trajectory for each arrival point $\underset{\sim}{x}$ are found by iteratively solving the equation

$$\underset{\sim}{\alpha} = \Delta t \underset{\sim}{v}(\underset{\sim}{x}-\underset{\sim}{\alpha}, t) \tag{3.5}$$

where $\underset{\sim}{v}$ in (3.5) is the *three*-dimensional wind field $(u, v, \dot{\eta})$. Since $\dot{\eta}$ was never explicitly required in the Eulerian version of the model (see Eqs. (2.18)-(2.19) for the Eulerian discretization of vertical advection), it is necessary to construct this field for the trajectory calculations. As $\dot{\eta}$ is already specified at the upper and lower boundaries ($\dot{\eta}=0$ at $\eta=0$ and at $\eta=1$), it would be natural to construct $\dot{\eta}$ at the half-levels (i.e., vertically staggered with respect to u and v), and indeed a preliminary version of the model was coded that way. However, it is more convenient to hold the three velocity components at the same set of points (which also coincide with the arrival points), so the formulation was changed to use $\dot{\eta}$ at the "full" levels. Thus, the vertical velocity used in (3.5) is defined by

$$\dot{\eta}_k = \frac{\frac{1}{2}\left[\left(\dot{\eta}\frac{\partial p}{\partial \eta}\right)_{k-\frac{1}{2}} + \left(\dot{\eta}\frac{\partial p}{\partial \eta}\right)_{k+\frac{1}{2}}\right]}{\left(\frac{\partial p}{\partial \eta}\right)_k} \tag{3.6}$$

where $\dot{\eta}\partial p/\partial \eta$ is already defined by (2.18) and

$$\left(\frac{\partial p}{\partial \eta}\right)_k = \frac{\Delta p_k}{\Delta \eta_k} = p_s \cdot \frac{\Delta A_k/p_s + \Delta B_k}{\Delta A_k/p_0 + \Delta B_k} \,. \tag{3.7}$$

In deriving (3.7) we have used (2.11) together with a formal definition of η itself (which

again was not required by the discretized Eulerian dynamics):

$$\eta_{k+\frac{1}{2}} = A_{k+\frac{1}{2}}/p_0 + B_{k+\frac{1}{2}} \qquad (3.8)$$

where p_0 is a constant pressure (chosen to be 1013.25 hPa).

The iterative procedure for solving (3.5) is analogous to that used by Ritchie (1991) in a σ-coordinate model. Given an estimate $\underset{\sim}{\alpha}^{(k)}$ after k iterations, the next iteration is given by

$$\underset{\sim}{\alpha}^{(k+1)} = \Delta t \underset{\sim}{v}(\underset{\sim}{x}-\underset{\sim}{\alpha}^{(k)}, t) \qquad (3.9)$$

where the vertical (η) component of the displacement is found first. The vertical component of $\underset{\sim}{\alpha}^{(k)}$ on the right-hand side of (3.9) is then updated before the horizontal components are found taking into account the spherical geometry following Ritchie (1987,1988). The first guess is given by

$$\underset{\sim}{\alpha}^{(0)} = \Delta t \underset{\sim}{v}(\underset{\sim}{x}, t) \ . \qquad (3.10)$$

The calculations include approximations to the spherical geometry away from the poles, following Ritchie and Beaudoin (1994). In agreement with previous work (reviewed by Staniforth and Côté 1991), little sensitivity was found to the order of interpolation used in the trajectory calculations, and linear interpolation appears to be sufficiently accurate. After providing a first guess via (3.10), a single further iteration was found to be adequate.

Once the midpoint $(\underset{\sim}{x}-\underset{\sim}{\alpha})$ of the trajectory has been found, the departure point $(\underset{\sim}{x}-2\underset{\sim}{\alpha})$ is immediately obtained (in the horizontal, the backward extension of the trajectory is along a great circle). In the vertical, if the departure point is then above the first (or below the last) model level, it is modified to lie on the first (last) level.

In solving (3.9), it is necessary to convert between a displacement in terms of the spatial coordinates and the corresponding displacement in terms of "gridlengths", in order to

select the correct three-dimensional block of points for the interpolation routine. This is simple in the horizontal, since the mesh length is constant in the λ-direction (at a given latitude), and almost constant in the θ-direction. It is more difficult in the vertical, where the grid spacing changes rapidly, and the conversion algorithm for the vertical displacement makes use of an auxiliary grid defined with high uniform resolution.

(c) "Non-interpolating" scheme in the vertical

An alternative formulation of the semi-Lagrangian scheme in three dimensions was suggested by Ritchie (1991). Equation (3.1) can be rewritten as

$$\frac{d_H X}{dt} + \dot{\eta}^* \frac{\partial X}{\partial \eta} = R - \dot{\eta} \frac{\partial X}{\partial \eta} + \dot{\eta}^* \frac{\partial X}{\partial \eta} \tag{3.11}$$

where

$$\frac{d_H X}{dt} \equiv \frac{\partial X}{\partial t} + A_H(X)$$

and A_H is the horizontal part of the advection operator defined in (2.27). In (3.11), $\dot{\eta}^*$ is defined to be a vertical velocity which would lead to the departure point of the trajectory at time $(t-\Delta t)$ lying exactly on a model level. This model level is chosen to be the one closest to the true departure point. Equation (3.11) is then approximated by

$$\frac{X^+ - X^-}{2\Delta t} = (R - \dot{\eta} \frac{\partial X}{\partial \eta})^0 + \dot{\eta}^* (\frac{\partial X}{\partial \eta})^0 \tag{3.12}$$

where the superscripts $+, 0, -$ respectively denote evaluation at the arrival point $(\underset{\sim}{x}, t+\Delta t)$, the midpoint $(\underset{\sim}{x}-\underset{\sim}{\alpha}, t)$ and the departure point $(\underset{\sim}{x}-2\underset{\sim}{\alpha}, t-\Delta t)$ of the *modified* trajectory. Since the modified departure point lies by definition on a model level, no vertical interpolation is required to evaluate X^-. As discussed in section 3(a) above, it is also possible

to evaluate the terms on the right-hand side of (3.12) by averaging the values at $(\underset{\sim}{x}-2\underset{\sim}{\alpha}, t)$ and $(\underset{\sim}{x}, t)$; in this case no vertical interpolation at all is required. Notice that a separate interpolation is required to evaluate the second term on the right-hand side of (3.12) since the quantity $\dot{\eta}^*$, defined by

$$\dot{\eta}^* = \frac{\eta^+ - \eta^-}{2\Delta t} \tag{3.13}$$

where η^+ and η^- are respectively the arrival and departure levels of the modified trajectory, is meaningful only at each gridpoint.

If the vertical velocity (or the timestep) is sufficiently small, then the modified departure point lies on the same model level as the arrival point, $\dot{\eta}^*$ is zero and the treatment of vertical advection becomes purely Eulerian. In general there is an Eulerian treatment of the advection by the "residual vertical velocity" $(\dot{\eta}-\dot{\eta}^*)$, which is small enough to guarantee that the Eulerian CFL criterion for vertical advection is respected. Thus, the "non-interpolating" scheme maintains the desirable stability properties of the "fully interpolating" scheme.

There is a subtle but important difference in the way the iterative scheme (3.9) is implemented to determine the modified trajectory in the non-interpolating scheme. As before, the first step at each iteration is to update the estimate of the vertical component of the displacement. The implied updated departure point is then moved to the closest model level. In the second step, the horizontal components are then updated using the winds evaluated at the midpoint of the *modified* trajectory. Notice that this gives a result different from that obtained by simply carrying out the trajectory calculation of the fully interpolating scheme and then projecting the departure point to the nearest model level. The modified procedure

described above is easily seen to be more consistent by considering the case in which the vertical velocity is not zero, but is small enough for the *modified* trajectory to be horizontal ($\dot{\eta}^*=0$). The discretization is then equivalent to a purely two-dimensional semi-Lagrangian scheme, the trajectory being computed using the horizontal wind field evaluated on a single model level.

An incidental advantage of the "non-interpolating" scheme over the "fully interpolating" scheme is that it resolves any ambiguities about the treatment of departure points above the top model level or below the bottom model level; the modified departure points automatically lie on the top or bottom level. The treatment of vertical advection becomes Eulerian, which is well-defined at the top and bottom levels. Thus, the non-interpolating scheme removes the need for artificial "nudging" of the departure points or extrapolation of quantities to points above or below the domain of the model levels.

Smolarkiewicz and Rasch (1991) have extended the principle of the "non-interpolating" semi-Lagrangian formulation to generate a broader class of stable and accurate advection schemes.

(d) Semi-Lagrangian discretization

Here we describe in detail only the fully interpolating version of the semi-Lagrangian discretization; the modifications necessary for the "non-interpolating in the vertical" version become evident by comparing the right-hand side of (3.12) with that of (3.2).

Following Ritchie (1988,1991), the momentum equations are integrated in *vector* form to avoid an instability of the metric term near the poles. Using the notation of (3.2) and defining the horizontal wind vector $\underset{\sim}{V}_H=(u, v)$, the semi-Lagrangian equivalent of (2.28)-(2.29) is

$$\frac{\underset{\sim}{V}_H^+ - \underset{\sim}{V}_H^-}{2\Delta t} + \left[f\underset{\sim}{k}\times\underset{\sim}{V}_H + \nabla\phi + R_d T_v \nabla \ln p \right]^0$$

$$= P_{\underset{\sim}{V}} + K_{\underset{\sim}{V}} - \frac{\beta}{2}\Delta_{tt}\nabla\left\{\underline{\underline{\gamma}}T + R_d T_r \ln p_s\right\} \tag{3.14}$$

where $\underset{\sim}{k}$ is the vertically directed unit vector and ∇ is the horizontal gradient operator in spherical coordinates. On the right-hand side of (3.14), $P_{\underset{\sim}{V}}$ and $K_{\underset{\sim}{V}}$ respectively denote the contributions of the physical parameterization schemes and horizontal diffusion, to be discussed in Section 3(f), while the semi-implicit correction terms are evaluated as in (3.4). For the momentum equations, it was found advantageous to evaluate the time-level t terms $[\ ]^0$ as an average between the values at the departure and arrival points of the trajectory, as in (3.3). The pressure gradient terms are discretized in exactly the same way as for the Eulerian model [see Section 2(b)].

Since (3.14) is in vector form, it is important to account for the change in the orientation of the coordinate system as the particle follows the trajectory; the manipulations required are as set out by Ritchie (1988) and simplified by Ritchie and Beaudoin (1994).

The thermodynamic and moisture equations (2.30)-(2.31) become

$$\frac{T^+ - T^-}{2\Delta t} - \left[\frac{\kappa T_v \omega}{(1+(\delta-1)q)p}\right]^0 = P_T + K_T - \frac{\beta}{2}\Delta_{tt}(\underline{\underline{\tau}}D) \ , \tag{3.15}$$

$$\frac{q^+ - q^-}{2\Delta t} = P_q + K_q \ . \tag{3.16}$$

In (3.15), the $[\ ]^0$ term is discretized as in (2.25), and evaluated at the midpoint of the trajectory, while the semi-implicit correction terms are evaluated as in (3.4).

The η-coordinate continuity equation (2.5) can be rewritten as

$$\frac{d}{dt}\left(\frac{\partial p}{\partial \eta}\right) + \frac{\partial p}{\partial \eta}\left(D + \frac{\partial \dot{\eta}}{\partial \eta}\right) = 0 . \tag{3.17}$$

Setting

$$p = A(\eta) + B(\eta) p_s$$

and noting that

$$\frac{\partial}{\partial t}\left(\frac{\partial A}{\partial \eta}\right) = \nabla .\left(\frac{\partial A}{\partial \eta}\right) = \frac{\partial p_s}{\partial \eta} = 0 ,$$

we also have

$$\frac{d}{dt}\left(\frac{\partial p}{\partial \eta}\right) = \frac{\partial B}{\partial \eta}\frac{dp_s}{dt} + \dot{\eta}\frac{\partial}{\partial \eta}\left(\frac{\partial p}{\partial \eta}\right) . \tag{3.18}$$

Combining (3.17) and (3.18),

$$\frac{\partial B}{\partial \eta}\frac{dp_s}{dt} + \frac{\partial p}{\partial \eta} D + \frac{\partial}{\partial \eta}\left(\dot{\eta}\frac{\partial p}{\partial \eta}\right) = 0 . \tag{3.19}$$

Now introducing the vertical discretization, (3.19) becomes

$$\Delta B_k \frac{dp_s}{dt} + \Delta p_k D_k + \left(\dot{\eta}\frac{\partial p}{\partial \eta}\right)_{k+\frac{1}{2}} - \left(\dot{\eta}\frac{\partial p}{\partial \eta}\right)_{k-\frac{1}{2}} = 0 , \tag{3.20}$$

the vertical discretization of $\dot{\eta}\partial p/\partial \eta$ having been defined in (2.18).

Changing the prognostic variable to $\ln p_s$,

$$\Delta B_k \frac{d}{dt}(\ln p_s) + \frac{1}{p_s}\left\{\Delta p_k D_k + \left(\dot{\eta}\frac{\partial p}{\partial \eta}\right)_{k+\frac{1}{2}} - \left(\dot{\eta}\frac{\partial p}{\partial \eta}\right)_{k-\frac{1}{2}}\right\} = 0 . \tag{3.21}$$

Combining (3.21) with the discrete definition of $\dot{\eta}\partial p/\partial \eta$ given by (2.18),

$$\Delta B_k \frac{d}{dt}(\ln p_s) - \Delta B_k \left\{ \frac{\partial (\ln p_s)}{\partial t} + \underset{\sim}{v}_k . \nabla \ln p_s \right\} = 0 \qquad (3.22)$$

where $\partial(\ln p_s)/\partial t$ is given by (2.14).

Noting that

$$\sum_{k=1}^{NLEV} \Delta B_k = 1 ,$$

and including the semi-implicit correction terms, the semi-Lagrangian discretization of the continuity equation finally becomes

$$(\ln p_s)^+ = \sum_{k=1}^{NLEV} \Delta B_k \left\{ (\ln p_s)^- + 2\Delta t \left(\frac{\partial (\ln p_s)}{\partial t} + \underset{\sim}{v}_k . \nabla \ln p_s \right)^0 \right.$$

$$\left. - \frac{\beta \Delta t}{p_s^r} \Delta_{tt} \left(\sum_{j=1}^{NLEV} (\Delta p_j^r D_j) \right) \right\} \qquad (3.23)$$

(Since there is no vertical advection term in (3.23), no modification is required for the vertically non-interpolating scheme). It is important to bear in mind that each contribution to the sum on the right-hand side of (3.23) involves a different trajectory. The interpolations for $(\ln p_s)^-$ and the semi-implicit correction terms are however two-dimensional, since these quantities are independent of vertical level. The $(\ )^0$ term is evaluated at the midpoint of the trajectory, and requires a three-dimensional interpolation.

In summary, the semi-Lagrangian discretization is given by Equations (3.14)-(3.16) together with (3.23).

(e) Comparison with other schemes

The semi-Lagrangian formulation presented above differs in some respects from those proposed by other authors. Perhaps the most notable difference lies in the treatment of the

conversion (ω) term in the thermodynamic equation (3.15), and of the right-hand side of the continuity equation (3.23). Both involve terms of the form $\underset{\sim}{v}.\nabla \ln p_s$, which in our scheme are computed in a purely Eulerian fashion. This may appear somewhat inconsistent; indeed McDonald and Haugen (1993) state as a specific design objective of their scheme that the operator $\underset{\sim}{v}.\nabla$ should not appear explicitly. The alternative approach, also taken by Williamson and Olson (1994), is to use the continuity equation in its semi-implicit semi-Lagrangian form to derive a consistent equation for *predicting* $\dot{\eta}\partial p/\partial \eta$, which can then be used to eliminate the $\underset{\sim}{v}.\nabla \ln p_s$ terms. In the σ-coordinate system, Bates et al. (1993) and McDonald and Haugen (1992) used a similar approach to derive a prognostic equation for $\dot{\sigma}$. A possible disadvantage of such an approach is that $\dot{\eta}\partial p/\partial \eta$ (or $\dot{\sigma}$) then follows an independent evolution, no longer satisfying a diagnostic relationship of the form (2.18). Our "Eulerian" treatment of the $\underset{\sim}{v}.\nabla \ln p_s$ terms avoids this disadvantage and seems to work well, but further study is required to determine whether this difference in formulation is important or not.

Another aspect of our semi-Lagrangian discretization of the continuity equation, which differs from that in other models, concerns the definition of the trajectory; in our scheme this is the same (three-dimensional) trajectory as used for the other variables. In the continuous form (3.19) of the equation, the advective part of the total derivative dp_s/dt may be regarded either as two-dimensional or as three-dimensional (since $\partial p_s/\partial \eta$ is zero). However the vertically discretized form (3.20) is well-defined only at discrete model levels, implying that for consistency the semi-Lagrangian discretization (3.23) should be based on *horizontal* trajectories. Correcting this inconsistency in our scheme by computing horizontal trajetories for the continuity equation, based on the horizontal wind at each model level, made very little difference to the results, and for the time being we have allowed the inconsistency to remain.

(As discussed later, in the case of the "vertically non-interpolating" scheme the modified trajectories are nearly always horizontal anyway.) In the case of the fully-interpolating scheme, recomputing the trajectories represents a significant expense; Bates et al. (1993) and McDonald and Haugen (1992) used a simple projection of the three-dimensional trajectory onto the model level of the arrival point. In our model this approach resulted in poor mass conservation, though Bates et al. (1993) came to the opposite conclusion. Again, the importance or otherwise of these differences in formulation is not yet firmly established.

(f) Time-stepping procedure

The general outline of the time-stepping procedure for the semi-Lagrangian version is similar to that described for the Eulerian model in Section 2(e). Thus at the start of a timestep, the model state at time $(t-\Delta t)$ is defined by the values of U, V, T, q and $\ln p_s$ on the Gaussian grid. To complete the semi-implicit corrections, the $(t-\Delta t)$ values of D, $\partial P/\partial\lambda$ and $\partial P/\partial\mu$ are also held on the grid. The model state at time t is defined by the spectral coefficients of ζ, D, T, q and $\ln p_s$. Legendre transforms followed by Fourier transforms are then used to compute D, U, V, T, $\partial T/\partial\mu$, q, $\partial q/\partial\mu$, $\ln p_s$ and $\partial(\ln p_s)/\partial\mu$ at time t on the model grid; additional Fourier transforms are used to compute the corresponding values of $\partial T/\partial\lambda$, $\partial q/\partial\lambda$ and $\partial(\ln p_s)/\partial\lambda$. Since ζ and the horizontal gradients of U and V are no longer required on the model grid, one multi-level Legendre transform and three multi-level Fourier transforms are saved in comparison with the Eulerian version.

Since the advection of moisture is handled by the semi-Lagrangian discretization (3.16), the horizontal gradients of q are only needed in order to compute the horizontal gradients of the virtual temperature T_v [which in turn are required to compute the $\nabla\phi$ term in (3.14)]. If T_v is chosen as the spectral variable as in section 2(h), these gradients are

available directly, and there is then no need to transform $\partial q/\partial\mu$ (or $\partial q/\partial\lambda$) to the model grid. The number of multi-level Legendre transforms per timestep is further reduced to 10. In passing, all the ingredients are then in place for a semi-Lagrangian treatment in which the moisture field is never transformed to spectral space (Williamson and Rasch, 1994), and only 8 multi-level Legendre transforms are required per timestep (compared with 17 in the original ζ-D Eulerian model).

After the transforms to the model grid, all the information is then available to compute the trajectories for each gridpoint, and to evaluate the "dynamical" contributions to the semi-Lagrangian discretization. Ignoring for a moment the contributions of the physical parameterization schemes and of the horizontal diffusion, each equation is either of the form

$$X^+(\underset{\sim}{x}) = X^-(\underset{\sim}{x}-2\underset{\sim}{\alpha}) + \Delta t\{R^0(\underset{\sim}{x}-2\underset{\sim}{\alpha}) + R^0(\underset{\sim}{x})\} + S^-(\underset{\sim}{x}-2\underset{\sim}{\alpha}) + S^+(\underset{\sim}{x}) \qquad (3.24)$$

or

$$X^+(\underset{\sim}{x}) = X^-(\underset{\sim}{x}-2\underset{\sim}{\alpha}) + 2\Delta tR^0(\underset{\sim}{x}-\underset{\sim}{\alpha}) + S^-(\underset{\sim}{x}-2\underset{\sim}{\alpha}) + S^+(\underset{\sim}{x}) , \qquad (3.25)$$

depending on whether the R^0 terms are averaged between the endpoints of the trajectory or evaluated at the midpoints. In (3.24) and (3.25), the S terms represent the semi-implicit corrections; S^- includes contributions from time-levels $(t-\Delta t)$ and t, while S^+ includes contributions from time-levels t and $(t+\Delta t)$.

In the first part of the calculation for equations of the form (3.24), the combined field $X^- + \Delta tR^0 + S^-$ is computed, and the value of this combined field at each departure point $(\underset{\sim}{x}-2\underset{\sim}{\alpha})$ is then found by interpolation. Adding the (uninterpolated) value of ΔtR^0 results in a provisional value of X^+ at each gridpoint, incorporating all the terms in (3.24) except for S^+. The calculation for equations of the form (3.25) proceeds similarly, except that two interpolations are required, one for $X^- + S^-$ at $(\underset{\sim}{x}-2\underset{\sim}{\alpha})$, and one for $2\Delta tR^0$ at $(\underset{\sim}{x}-\underset{\sim}{\alpha})$.

A provisional value X^+ is now available at each gridpoint for each variable, and is

used together with X^- at the same gridpoint to compute an "Eulerian" tendency. These fields and their tendencies are then supplied to the physical parameterization routines, which increment the tendencies with their respective contributions, just as in the Eulerian version (except that, to avoid extra interpolations, the S^- terms have been included in the supplied dynamical tendencies). If T_v is chosen as the spectral variable, a provisional value of T_v^+ is computed at this point.

The contributions from the S^+ terms at time t are now added in, resulting in a set of equations of the form

$$U^+ + \frac{\beta \Delta t}{a} \frac{\partial P^+}{\partial \lambda} = Q_1 \tag{3.26}$$

$$V^+ + \frac{\beta \Delta t}{a} \cos\theta \frac{\partial P^+}{\partial \theta} = Q_2 \tag{3.27}$$

$$T^+ + \beta \Delta t \underline{\tau} D^+ = Q_3 \tag{3.28}$$

$$q^+ = Q_4 \tag{3.29}$$

$$(\ln p_s)^+ + \beta \Delta t \underline{\nu} D^+ = Q_5 \tag{3.30}$$

where the right-hand sides Q_1-Q_5 include all the terms which have been computed on the grid, and T_v^+ replaces T^+ if T_v is the spectral variable. Equations (3.26)-(3.30) have exactly the same form as Equations (2.37)-(2.41) of the Eulerian model and are solved in exactly the same way, by first transforming to spectral space. After finding the new spectral coefficients at time $(t+\Delta t)$, horizontal diffusion is also applied in the same way as for the Eulerian version.

The implementation of the time-filtering for the semi-Lagrangian model is identical to that for the Eulerian version, as described in Section 2(f).

(g) Optimization of vertically non-interpolating scheme

In the "vertically non-interpolating" scheme, the departure point of each modified trajectory lies on a model level. For the set of arrival points on each model level, it is of interest to determine the frequency distribution of the corresponding departure points. The results of an experiment run to collect these statistics led to a significant optimization of the code for the vertically non-interpolating scheme.

The statistics were obtained from a 10-day forecast using the model in its operational configuration: T213, 31 levels, with a 15-minute timestep. The results are summarized in Table 1, which shows that the vast majority (99.67% overall) of modified trajectories are horizontal; no departure point was ever more than three model levels away from its corresponding arrival point.

The implication of these results is that a great deal of redundant calculation was being performed in the vertically non-interpolating scheme. For each horizontal modified trajectory, the interpolation of the horizontal winds in the trajectory calculation itself becomes two-dimensional rather than three-dimensional, as do the interpolations of "right-hand side" terms at the midpoint of the trajectory, while the additional interpolations to calculate terms of the form $\dot{\eta}^{*}(\partial X/\partial\eta)^{0}$ in (3.12) are not required at all. Consequently, special routines were written to perform interpolations which are two-dimensional everywhere except at a set of "flagged" points where they become three-dimensional, and similarly to perform two- or three-dimensional interpolations at the flagged points while skipping all other points. The use of these special routines reduced the "semi-Lagrangian overhead" for the vertically non-interpolating scheme by about 30%.

TABLE 1

Frequency distribution (%) of departure points in the 'vertically non-interpolating' scheme (* indicates <0.005%)

Arrival level k	Departure levels k	$k\pm1$	$k\pm2$	$k\pm3$
1-6	100.00	-	-	-
7-9	100.00	*	-	-
10	99.99	0.01	*	-
11	99.96	0.04	*	-
12	99.89	0.11	*	-
13	99.76	0.24	*	*
14	99.60	0.40	*	*
15	99.43	0.57	*	*
16	99.28	0.72	*	-
17	99.16	0.83	0.01	-
18	99.08	0.92	*	-
19	99.05	0.94	0.01	-
20	99.05	0.94	0.01	*
21	99.09	0.91	*	*
22	99.14	0.85	0.01	*
23	99.22	0.78	*	-
24	99.31	0.69	*	-
25	99.44	0.56	*	-
26	99.60	0.40	*	-
27	99.78	0.22	*	-
28	99.92	0.08	*	-
29	99.99	0.01	-	-
30	100.00	*	-	-
31	100.00	-	-	-

TABLE 2

Analysis of CPU time (%)

	Eulerian	Fully interpolating semi-Langrangian	Vertically non-interpolating sem-Langrangian
Dynamics	21	15	17
Physics	53	42	45
FFT	6	3	4
Legendre transforms	20	13	14
Semi-Langrangian	-	27	20

4. Computational details

Implementing a high-resolution model, which must run operationally within a given elapsed time on a given computer system, presents a number of interesting technical challenges. In this section we present some of the computational details which enabled the goal of implementation to be achieved.

(a) Scanning structure

Each timestep of the model integration procedure consists of three scans.

At the beginning of the timestep, the model fields at time $(t-\Delta t)$ are specified in gridpoint form (as described in Section 2(f), these fields are "partially time-filtered"). The gridpoint values of the model variables are contained in a "gridpoint workfile", held on a secondary storage device and organized as a random-access file with one record for each latitude row. Meanwhile, the model fields at time t are specified in spectral form, all the spectral coefficients being held in central memory. The first scan consists of Legendre transforms to compute the Fourier coefficients of the model variables at time t on each latitude row, the results being written out to a "Fourier workfile", again organized with one record for each latitude row. During the first scan, latitude rows are processed in north/south pairs with the members of each pair being equidistant from the equator, in order to make use of the symmetries of the Legendre polynomials (see for example Temperton,1991). Once this first scan has been completed, the spectral coefficients are no longer required and the central memory arrays can be released for use during the next scan.

The second scan steps through the latitude rows, starting at the row nearest the North Pole and proceeding southwards. At each row, the corresponding records of the gridpoint values at time $(t-\Delta t)$ and the Fourier coefficients at time t are read in. Fourier transforms then provide gridpoint values of the fields (together with any required horizontal derivatives)

at time t. At this juncture, the time-filtering of the fields at time $(t-\Delta t)$ is completed, while "partially time-filtered" fields at time t are also computed and written out to the gridpoint workfile ready for the next timestep.

The gridpoint calculations for the present timestep continue using the time-filtered values at $(t-\Delta t)$ and the unfiltered values at time t. The right-hand sides of the equations, discretized in semi-Lagrangian form as in Section 3, are computed with terms being grouped separately depending on whether they will be evaluated at the departure point, the midpoint or the arrival point of the trajectory. The results of these calculations, together with the horizontal wind components and the vertical velocity $\dot{\eta}$, are then stored in a "rotating buffer" which contains values for a number of consecutive latitude rows. The gridpoint calculations described so far correspond to the southernmost row contained in this buffer. Next, the focus of the computation returns to the *central* row of the buffer. Values of the wind fields and the right-hand sides of the equations are now available at a sufficient distance to the north and south of the central row for the trajectory calculations to be performed and for the semi-Lagrangian timestep to be implemented, thus furnishing provisional values at $(t+\Delta t)$. As described in Section 3(d), the contributions from the physical parameterization schemes can then be incorporated to complete the calculation of the right-hand sides Q_1-Q_5 of Eqs. (3.26)-(3.30).

These right-hand sides are now Fourier transformed and the coefficients are written out to another Fourier workfile, again organized with one record for each latitude row but this time with a special structure which will be exploited in the third scan. The computation then proceeds southwards to the next pair of "southernmost" and "central" rows, the values computed for the new southern row overwriting those in the buffer for the previous northernmost row, which are no longer required.

At the start of the second scan, there is clearly an initialization phase during the first few rows when only the first part of the above calculations can be done. Similarly, at the end of the scan there is a "winding-down" phase during which the first part of the calculations has already been done, and only the second part is required. The same logical structure is also used to run the Eulerian version of the model, but in this case the width of the "rotating buffer" can be reduced to that for a single latitude row.

The third scan performs direct Legendre transforms to obtain the provisional spectral coefficients at time $(t+\Delta t)$ from the Fourier coefficients computed in the second scan, using Gaussian quadrature. The calculation proceeds one zonal wavenumber at a time. Here we make use of the special structure of the Fourier workfile; although the file was written row by row, it can be read in "transposed" fashion, wavenumber by wavenumber. The direct Legendre transforms first exploit the symmetries of the Legendre polynomials, and then complete the calculations using highly efficient matrix multiplication routines. To see how this is achieved, notice that since a single Legendre transform can be written as a matrix/vector multiplication of the form $\underset{\sim}{y}=\underline{\underline{P}}\underset{\sim}{x}$, a set of simultaneous transforms for the same zonal wavenumber but for different variables and model levels can be written as

$$[\underset{\sim}{y}_1 \; \underset{\sim}{y}_2 \; \cdots \; \underset{\sim}{y}_N] = \underline{\underline{P}} \, [\underset{\sim}{x}_1 \; \underset{\sim}{x}_2 \; \cdots \; \underset{\sim}{x}_N]$$

which is indeed in the form of a matrix multiplication $\underline{\underline{Y}}=\underline{\underline{P}}\underline{\underline{X}}$. A similar technique could have been used in the first scan, and this has been incorporated in the latest version of the model.

After the transformation to spectral space, the semi-implicit equations are solved and the horizontal diffusion is implemented as described in Section 2(e), thus completing the calculation of the spectral coefficients at time $(t+\Delta t)$. At the end of the third scan, the whole model has been advanced by one timestep.

(b) Multitasking

Currently the model is run on a "modestly parallel" supercomputer (specifically, a Cray Y-MP C90 with 16 processors), and multitasking is an important aspect of the strategy to make the best use of the available computer power. We have chosen to rely mainly on high-level "macrotasking", i.e., dividing the computation into large independent units of work, each of which is assigned to one of the processors. Here only a brief outline will be given; additional details and discussion are provided by Dent (1992).

In the first scan, the unit of work is a pair of latitude rows. Each pair is independent of all the others, and a simple dynamic scheduling technique can be used: as each processor becomes free, a new pair of rows is assigned to it.

In the second scan, the unit of work is a single latitude row. For the semi-Lagrangian version, the calculations for each row are no longer independent of those for all the other rows. The trajectory calculations and semi-Lagrangian advection algorithm for the central row of the rotating buffer can only be carried out once the required calculations have been completed for all the neighbouring rows, and somewhat complex logic is required to control the multitasking during this scan.

In the third scan, the unit of work is a single zonal wavenumber. Each wavenumber is independent of all the others, and the scheduling technique used in the first scan can again be used. The work content of each wavenumber varies from a maximum at m=0 to a minimum at the largest value of m (the "tip" of the triangular truncation), and the dynamic scheduling technique is effective in spreading the work over available processors.

(c) Performance

The following performance figures relate specifically to the operational version of the model run at horizontal resolution T213 with 31 levels on the 16-processor Cray Y-MP C90. With the model timestep set at 15 minutes the total CPU time per forecast day would be

about 1.5 hours on a single processor, the corresponding elapsed time (excluding the post-processing) being 7 minutes when the work is shared amongst 16 processors. This represents a sustained computation speed of about 3.5 gigaflops (3.5×10^9 floating-point operations per second). The memory requirements are 49 Mwords of central memory plus 70 Mwords of secondary storage. Multitasking using 16 processors provides a speedup factor of 13 compared with using a single processor. A typical operational 10-day forecast, including all the post-processing, takes 2 hours of elapsed time.

(d) Analysis of CPU time

In developing a high-resolution spectral model, the cost of the transforms (particularly the Legendre transforms) may be a cause for concern (e.g., Côté and Staniforth, 1990). In the case of a semi-Lagrangian model, it is clearly important that the gain obtained through the use of longer timesteps is not outweighed by the extra cost of the semi-Lagrangian scheme. In view of these concerns, it is of interest to analyse the CPU time required for our model. Table 2 shows the percentage breakdown for the Eulerian version, for the fully interpolating semi-Lagrangian scheme and for the vertically non-interpolating scheme, at T213/L31 resolution.

This analysis suggests that the spectral method is still perfectly viable at this resolution, and that considerably higher resolutions can be achieved before the cost of the transforms becomes a matter for serious concern. The overhead of the semi-Lagrangian scheme, particularly the non-interpolating version, is also quite modest; for the present resolution it permits a timestep of 15 minutes compared with 3 minutes for the Eulerian version, and the resulting reduction in the CPU time for the forecast is about a factor of four. The semi-Lagrangian overhead is in fact slightly less than suggested by the figures in Table 2, since there is a simultaneous reduction in the number of transforms compared with the Eulerian scheme. Comparing the two variants of the semi-Lagrangian scheme, the overall

CPU time for the non-interpolating version is 8.5% less than that for the fully interpolating version.

(e) The IFS model

On 2nd March 1994, the model code described above was replaced in operations by the IFS ("Integrated Forecasting System") model, developed in collaboration with Météo-France (where it is known as ARPEGE; see Courtier et al. (1991) for an account of this project). The new code includes all the features required for three- and four-dimensional variational data assimilation (Thépaut and Courtier, 1991; Rabier and Courtier, 1992), and for determining optimal unstable perturbations for ensemble prediction (Buizza et al., 1993). The computational structure of the forecast model component of the system is similar to that described above but includes further improvements in efficiency, notably the matrix-multiplication treatment of the Legendre transforms in the first scan as well as the third scan (see section 4(a) above), and the option to combine several latitude rows together (for example near the poles of the reduced grid) resulting in longer vectors.

5. Experimental Results

(a) Basic model configuration

Unless otherwise stated, the experiments reported on here were performed with a high resolution version of the ECMWF forecast model having a spectral representation in the horizontal with a triangular 213-wave truncation (T213), and 31 levels in the vertical (L31) as indicated in Fig.1. The baseline semi-Lagrangian version is the "vertically non-interpolating" scheme (see section 5(e)) which has been used operationally at ECMWF since August 1992.

The orography for the T213 model is derived from the U.S. Navy data set. The mean and variance of the height are first computed over the area represented by each point of the Gaussian grid, and an "envelope" orography is constructed by adding one standard deviation to the mean at each point (Jarraud et al.,1988). A Gaussian filter of radius 25km is then applied, and finally the resulting orography is spectrally fitted. The orography for the T106 model was derived in exactly the same way, except that the radius of the Gaussian filter was 50km.

The noise characteristics of the semi-Lagrangian versions were found to be sensitive to the evaluation of the right-hand-side terms of the governing dynamical equations (see also Tanguay et al., 1992). It was found to be important to calculate the momentum-equation terms as averages of values at the beginning and end points of the trajectories. However, applying this spatial averaging to the temperature and continuity equations turned out to degrade the results slightly. Here the right-hand-side terms for the temperature and continuity equations are calculated at the mid-points of the trajectories. The classical semi-implicit scheme is used (see the discussion following (2.31)), except as noted in section 5(c).

The model includes a sophisticated set of parameterization schemes, including

radiation (Morcrette, 1990), a diagnostic cloud scheme (Slingo, 1987), a mass-flux convection scheme (Tiedtke, 1989), vertical diffusion based on the formulation of Louis (1979), gravity-wave drag (Miller et al., 1989), large-scale precipitation, and surface processes (Blondin and Böttger, 1987).

Three parameterization changes were found to be necessary during the course of the development of the semi-Lagrangian model versions. The need for the first, reported by Janssen et al. (1992), had in fact been identified in Eulerian T106/L19 forecasts in which a time-truncation error in the parameterization of boundary-layer diffusion caused low-level winds to be generally stronger in forecasts with a 15-minute timestep than in forecasts with much shorter timesteps. The error arose because the time-split implicit solution used for the boundary-layer parameterization did not successfully preserve the balance between the resolved dynamical forcing and the turbulent diffusion. The semi-Lagrangian versions of the model, and the $U-V$ Eulerian version, produce full dynamical tendencies in grid-point space which were not directly available to the parameterization in the original $\zeta-D$ Eulerian version. The time-truncation error has been reduced by incorporating these dynamical tendencies in the solution of the implicit equations for the diffusive boundary-layer tendencies. This was necessary to get good agreement between the 10m wind forecasts produced by Eulerian and (longer-timestep) semi-Lagrangian versions.

The other two parameterization changes relate to the computational stability of the model when long timesteps are used. It was found necessary to replace explicit time-stepping in the parametrization of gravity-wave drag by an implicit treatment similar to that applied to boundary-layer diffusion. Stabilization of the convective mass-flux parameterization was achieved by artificially limiting the mass fluxes when a CFL-type stability criterion was breached. These changes also had a beneficial effect on the computational stability of the

Eulerian versions of the model. Without them, a timestep no longer than three minutes had to be used for stable integrations at T213/L31 resolution, whereas we shall see later that longer timesteps can now be used provided the basic dynamical advection scheme does not cause instability.

The experiments reported below use horizontal diffusion and time filtering similar to those employed operationally since August 1992. The coefficient of the fourth-order horizontal diffusion operator ($0.2937 \times 10^{15} m^4 s^{-1}$, see equation (2.46)) applied at T213 resolution corresponds to an e-folding time of 0.75h on the shortest-resolved scale. The Eulerian integrations reported here all make use of artificially enhanced horizontal diffusion at upper levels and for strong wind-speeds. This was originally adopted operationally for T106 resolution to ensure computational stability using a 15-minute timestep (Simmons et al., 1989). The artificial enhancement has been almost completely removed both for the semi-Lagrangian integrations described here and for operational use of the semi-Lagrangian versions. Enhanced damping was kept only for divergence close to the top of the model. This was because tests with no enhancement gave noise in the divergence and temperature fields along a $130 ms^{-1}$ jet at 10hPa over the Antarctic in a forecast from 28 July 1991.

A time-filtering parameter (see section 2(f)) of 0.1 was used for all experiments reported here. This is the value used operationally at present, and previously used operationally for T106 Eulerian forecasts.

Mass conservation is not guaranteed even by the Eulerian version of the model, since $\ln p_s$ is used as the spectral variable. In practice this is not a problem; during the course of an operational 10-day semi-Lagrangian T213 forecast the mean surface pressure normally varies by less than 0.5hPa, and in fact the mass conservation is rather better than it was for the previously operational Eulerian T106 model.

The physical parameterizations employed in these experiments form the set that was in use operationally from August 1992 to February 1993, when a significant improvement was made to the radiation code. The latter change in particular addressed some problems seen in the meteorological performance of the 31-level version of the model. For this reason, and since the 31-level resolution shows particular benefit in data assimilation experiments which are beyond the scope of this paper, we do not show any comparison of 19- and 31-level results in the following sections.

In order to assess the impact of various numerical parameters and formulations, sets of integrations were performed for 12 independent cases starting from operational analyses on the 15th of each month during the first year following the implementation of the T213/L31 model on September 17, 1991. The following figures compare the skill (averaged over the 12 cases) obtained with a control version and an experimental version of the model.

(b) Eulerian versus semi-Lagrangian formulation

The main motivation for using a semi-Lagrangian formulation is to permit the use of time steps that far exceed the Courant-Friedrichs-Lewy (CFL) stability criterion for the corresponding Eulerian model, thus enhancing the model efficiency, provided that the additional time truncation error does not significantly decrease the accuracy. Figure 3 shows the mean objective scores for the northern hemisphere comparing the Eulerian version with a 3 minute timestep (solid) and the semi-Lagrangian version with a 15 minute timestep (dashed). Figure 4 shows the corresponding result for the southern hemisphere. It is seen that the accuracies are almost equivalent, particularly for forecasts whose skill exceeds the 60% threshhold. Thus, even at this high resolution, the semi-Lagrangian scheme permits a fivefold increase in timestep with no significant degradation in the quality of the forecasts. In section 4(d) it was seen that the overhead of the semi-Lagrangian scheme is approximately

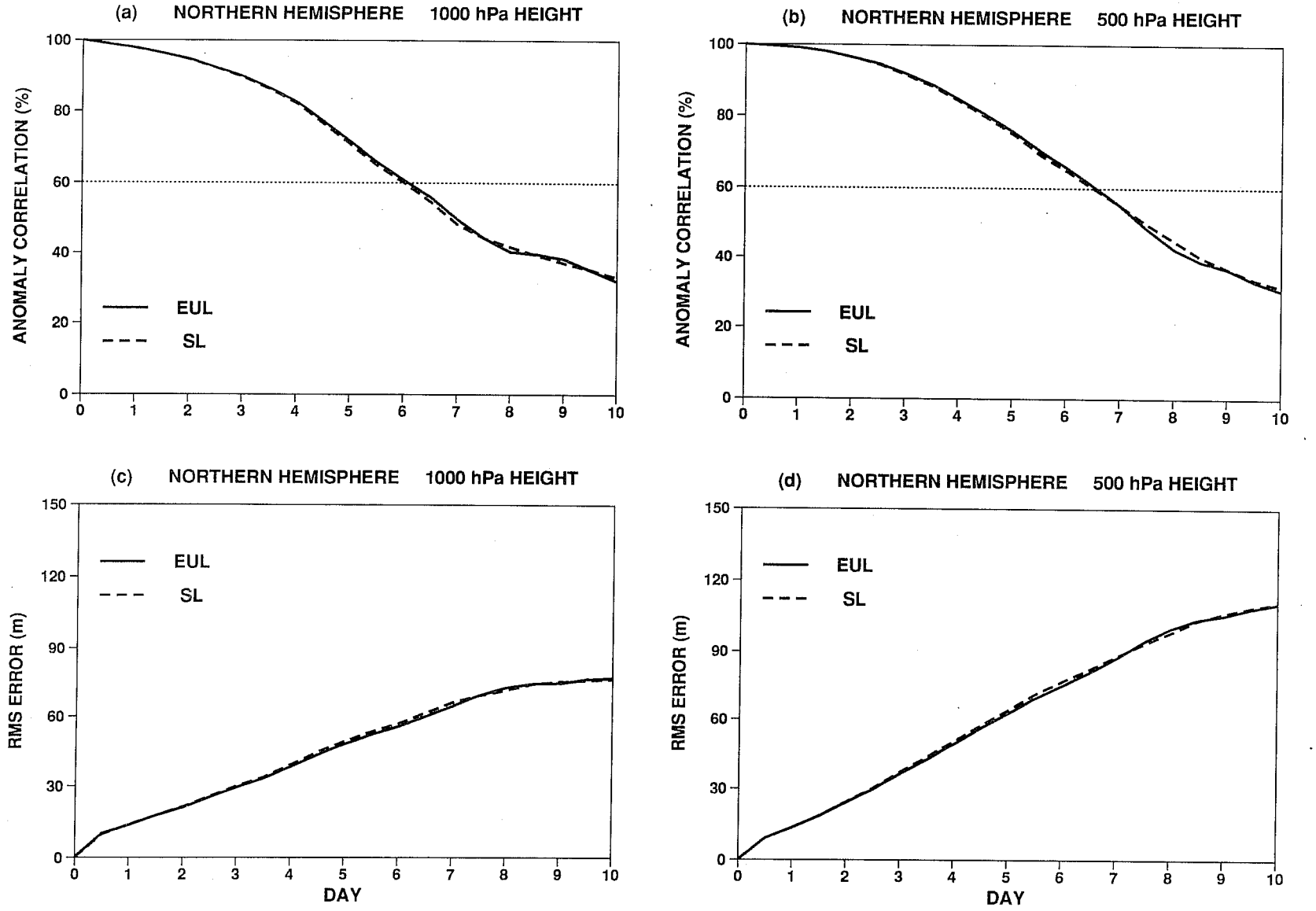

Fig. 3 Mean objective scores for the northern hemisphere comparing the Eulerian versionwith a 3 min timestep (solid) and the (vertically non-interpolating) semi-Lagrangian version with a 15 min timestep (dashed):

(a) anomaly correlation of 1000 hPa height (b) anomaly correlation of 500 hPa height

(c) root-mean-square error of 1000 hPa height (metres) (d) root-mean-square error of 500 hPa height (metres).

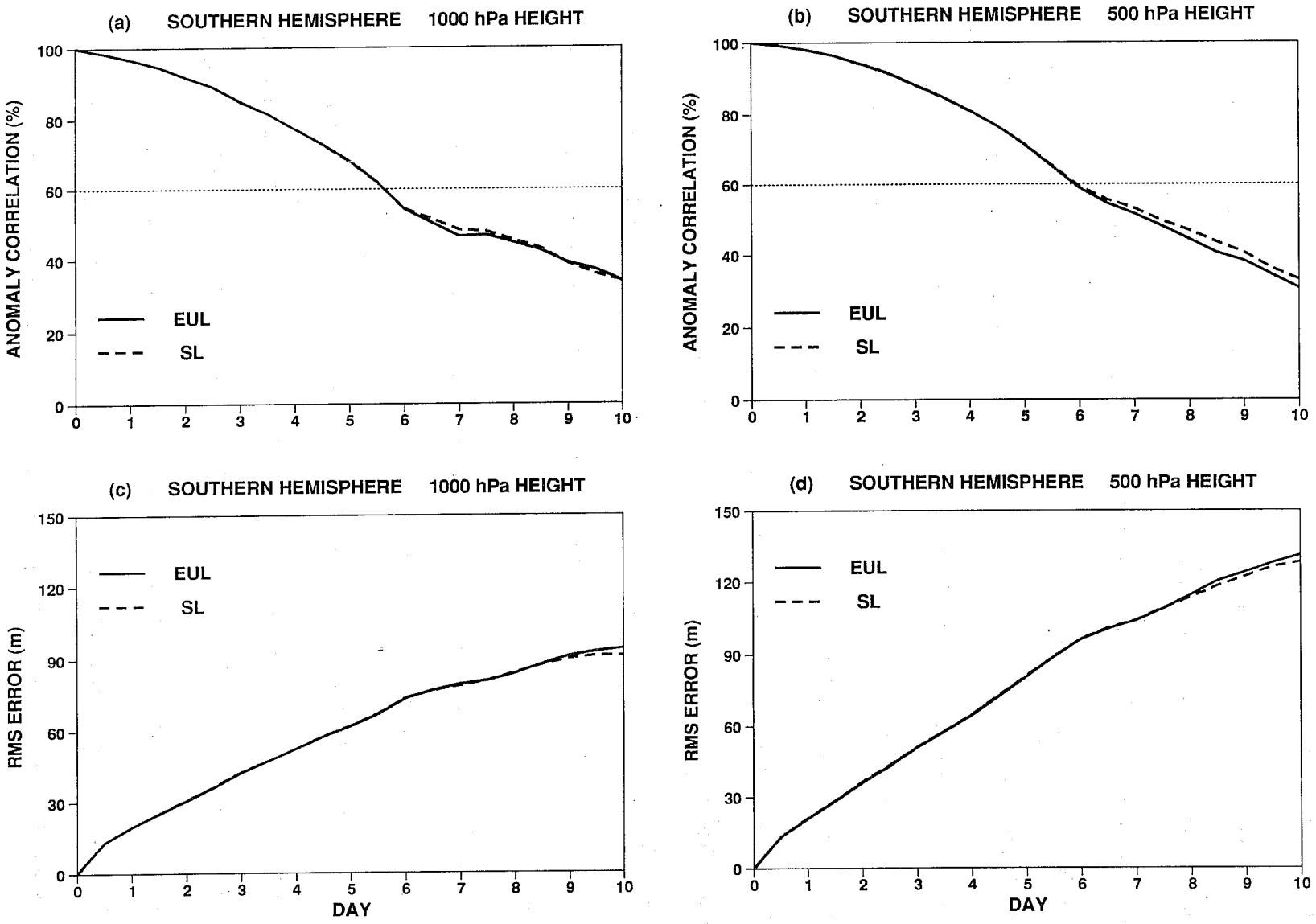

Fig. 4 As in Fig. 3 except for southern hemisphere.

20%, so the semi-Lagrangian version gives an efficiency improvement of about a factor of four relative to the Eulerian in this particular comparison.

(c) Impact of increasing timestep

In section 5(b) the Eulerian model used a timestep of 3 minutes and the semi-Lagrangian model was integrated with a 15 minute step under the basic configuration described in section 5(a). Given the parameterization changes discussed earlier, both versions can actually run stably with longer timesteps. For example, the flow and timestep dependent horizontal diffusion used in the Eulerian model has enabled the set of 12 cases to be integrated stably with a timestep of 7.5 minutes. Figures 5(a) and (b) show the impact of the change in timestep on the mean anomaly correlations of the northern hemisphere geopotential heights at 1000 hPa and 500 hPa respectively. Figures 5(c) and (d) present the corresponding impact on the root-mean-square errors. These results show that the accuracies are equivalent, especially when the anomaly correlation exceeds the 60% threshold. However, it should be noted that, although the enhanced diffusion has successfully inhibited the CFL instability in these 12 cases with the 7.5 minute timestep, instability has been found to occur with larger timesteps.

Similarly, the 15 minute timestep used with the semi-Lagrangian version is somewhat conservative. Figure 6 shows that there is negligible impact on the scores if the timestep is increased to 20 minutes. The 12 cases have also recently been run successfully with a 22.5 minute timestep in a semi-Lagrangian version. For these forecasts the semi-implicit parameter β (see the discussion following 2.31) was increased from 1 to 1.5. This version is now being used operationally at ECMWF to produce 3-day forecasts from 00Z data in order to produce boundary conditions requested by member states for limited area models. The increased value of β enhances the semi-implicit stability with the larger timestep, as analysed by Simmons

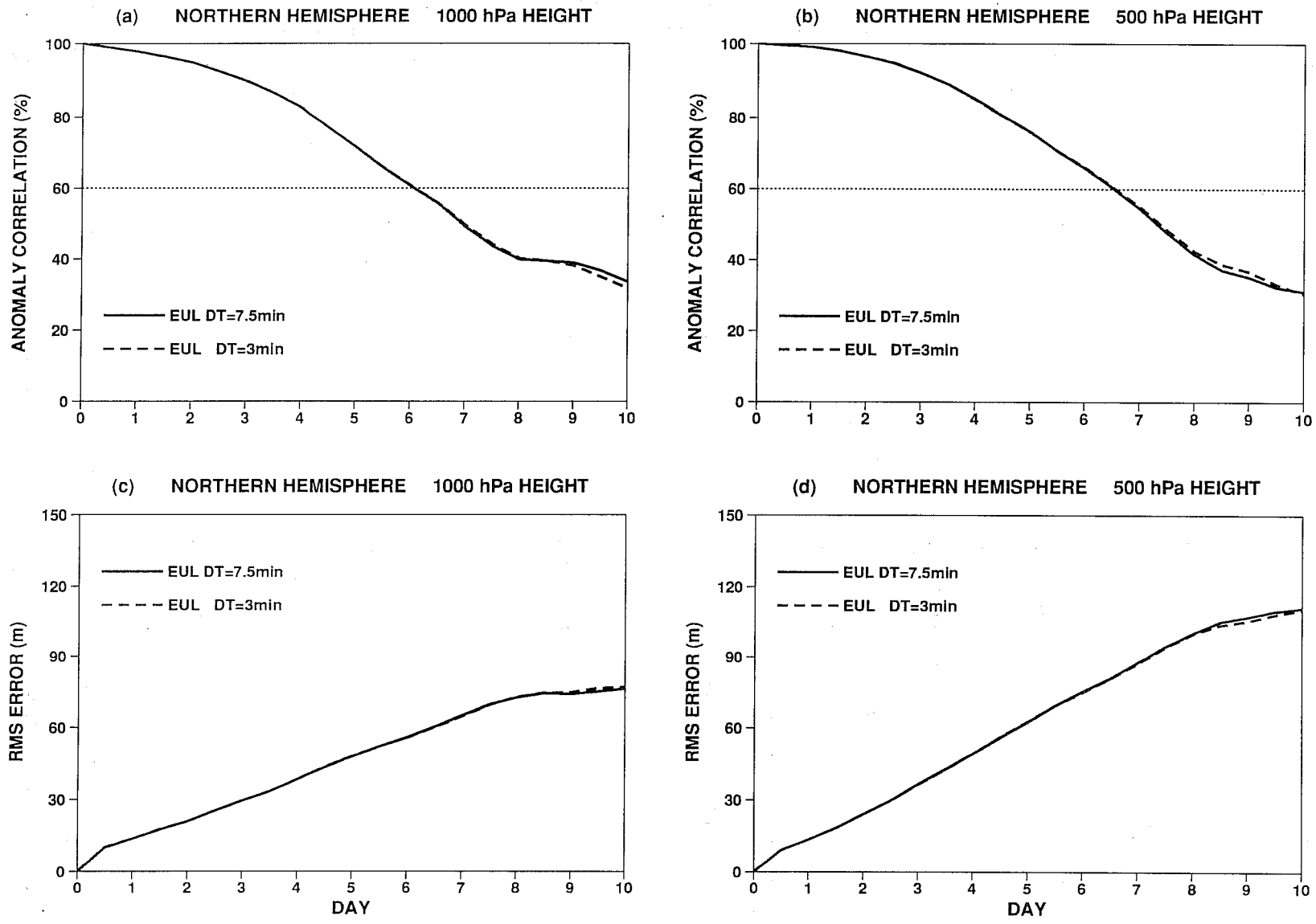

Fig. 5 Mean objective scores for the northern hemisphere for the Eulerian model comparing a 3 min (solid) and a 7.5 min (dashed) timestep:
(a) anomaly correlation of 1000 hPa height (b) anomaly correlation of 500 hPa height
(c) root-mean-square error of 1000 hPa height (metres) (d) root-mean-square error of 500 hPa height (metres).

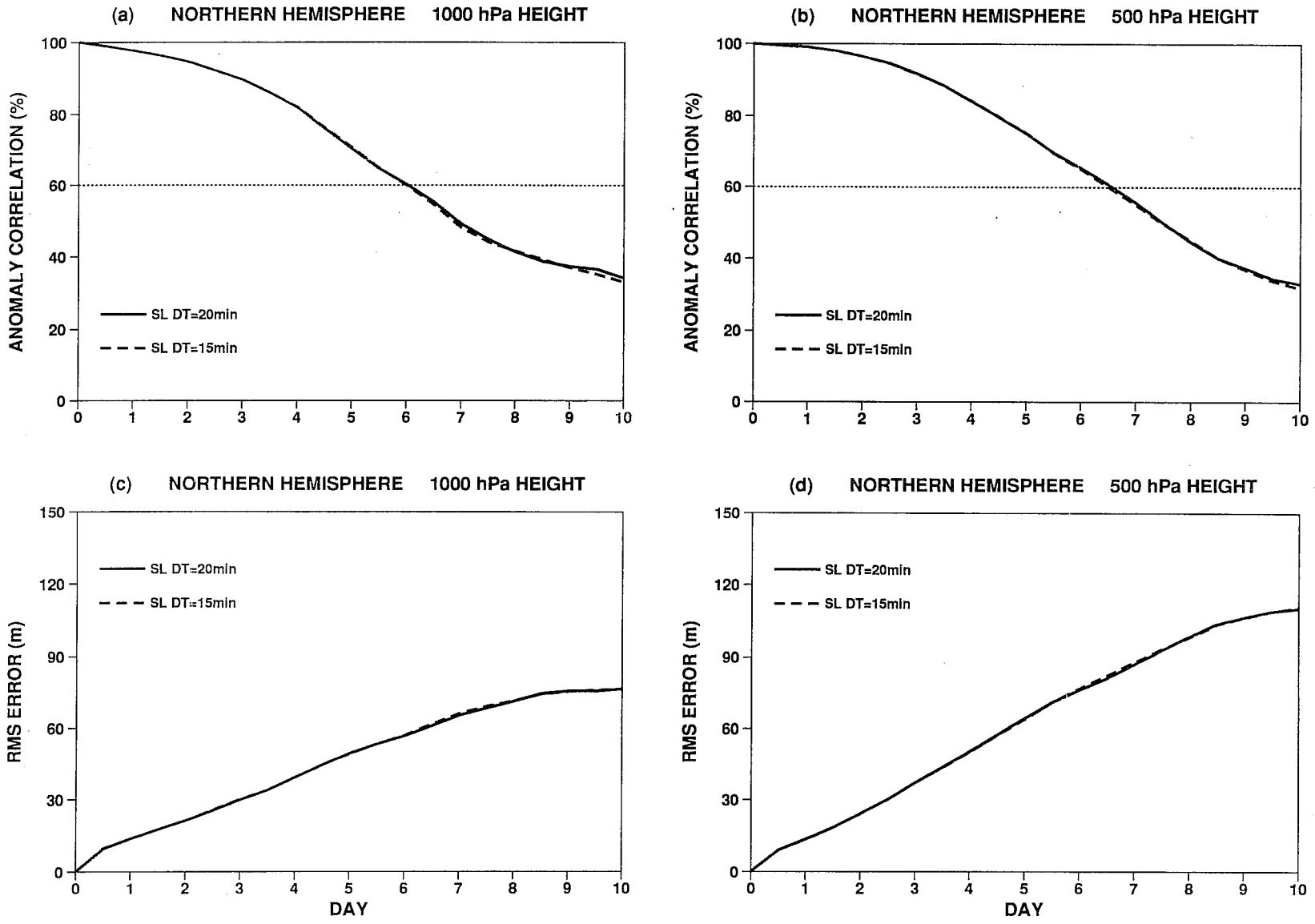

Fig. 6 Mean objective scores for the northern hemisphere for the (vertically non-interpolating) semi-Lagrangian model comparing a 20 min (solid) and a 15 min (dashed) timestep:
(a) anomaly correlation of 1000 hPa height (b) anomaly correlation of 500 hPa height
(c) root-mean-square error of 1000 hPa height (metres) (d) root-mean-square error of 500 hPa height (metres).

et al. (1978). It is largely for concerns about the accuracy of the physical parameterization and the amount of noise near orography that the 15 minute timestep is currently still retained for the operational 10-day forecasts.

(d) Hybrid versus sigma vertical coordinate

An important aspect of sections 2 and 3 is the formulation of a hybrid coordinate discretization which is suitable for a semi-Lagrangian treatment. A sigma-coordinate version of the model is available as a simplification of the hybrid coordinate code. The semi-Lagrangian algorithms used here were prepared as an extension of those used by Ritchie (1991) in a finite element discretization in a sigma coordinate. As a test of this extension, the hybrid coordinate code was run in sigma-coordinate mode. A selection of scatter plots of northern hemisphere anomaly correlations for the 12 cases comparing sigma- and hybrid-coordinate T213/L31 forecasts is shown in Figure 7. Panels (a) and (b) establish that the hybrid coordinate version performs as well as the sigma-coordinate configuration in the troposphere, where the two coordinates should agree fairly closely with each other. Panels (c) and (d) show that the hybrid coordinate results are systematically better than those for the sigma coordinate in the stratosphere. Hence the design advantage of the hybrid coordinate is maintained even in this high resolution semi-Lagrangian application. Visual examination of the 10 hPa height maps for individual cases (not shown) reveals that there is less noise over mountainous regions with the hybrid coordinate version. It is worth noting that no special filters were required in order for this application of the semi-Lagrangian method in hybrid coordinates to work successfully in a three time-level model, contrary to the experience reported by McDonald and Haugen (1993) for their application in a two time-level model.

(e) Impact of the "vertically non-interpolating" scheme

The T213/L31 model was implemented operationally in September 1991 using the

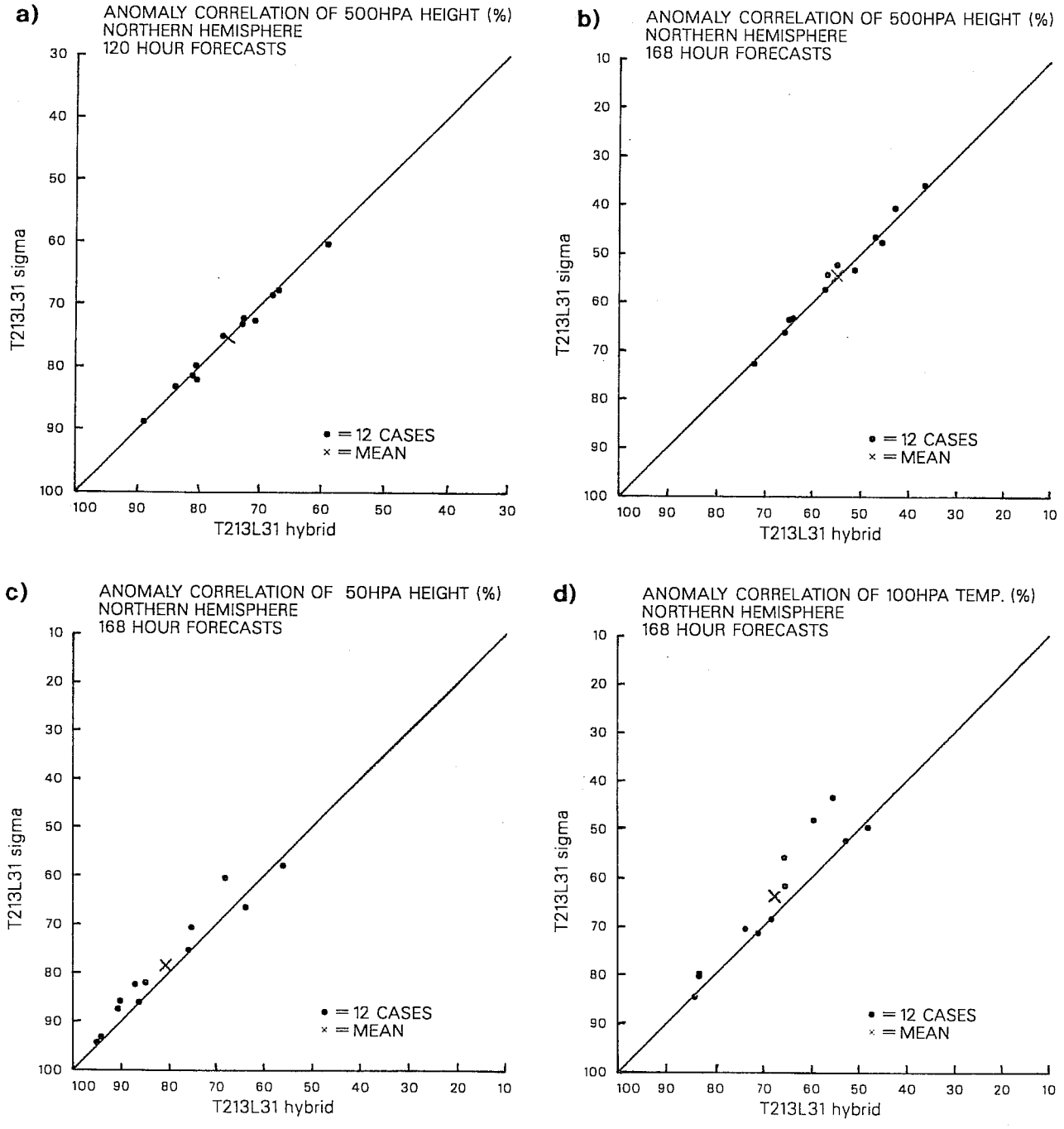

Fig. 7 A selection of scatter plots of northern hemisphere anomaly correlations for 12 cases comparing sigma- and hybrid-coordinate forecasts using T213/L31 resolution and semi-Lagrangian advection:

(a) 500 hPa height at 120 hours
(b) 500 hPa height at 168 hours
(c) 50 hPa height at 168 hours
(d) 100 hPa temperature at 168 hours.

"fully interpolating" version of the semi-Lagrangian scheme. The higher resolution version immediately demonstrated clear improvements in the forecasts in the first few days of the 10-day forecast range. However, despite extensive parallel testing before implementation, during the subsequent months it was found that, relative to the former operational model, there was increased day-to-day variability in the forecasts in the medium-range. The levels of eddy kinetic energy were typically higher with this version, too. Lower kinetic energy levels were also found in Eulerian versions of the T213/L31 model. Following several studies to try to determine which aspects of the semi-Lagrangian formulation were responsible for this behaviour, attention focussed on the option of using the "vertically non-interpolating" scheme (Ritchie, 1991) which had been in use operationally in the 21 sigma level semi-Lagrangian Canadian spectral model since its implementation in March 1991. This scheme was included quite early on in the Centre's semi-Lagrangian code, but was not fully validated during the development of the code because it was not expected to be necessary at the higher vertical resolution.

Tests of this option revealed a positive impact on objective measures of skill. This is evident in the anomaly correlations at 1000 hPa and 500 hPa for the northern hemisphere (Figures 8(a) and (b)), as well as in the corresponding root-mean-square height errors (Figures 8(c) and (d)). The improvement is even more striking in the results for the European region, as seen in Figure 9. Moreover, levels of eddy activity are generally lower with this version than with the fully interpolating scheme. Two synoptic examples are shown in Figure 10. The predominant occurrence of positive forecast height differences near the bases of troughs and cut-off lows indicates that the vertically non-interpolating scheme reduces the tendency of the model to produce troughs and cut-offs that are too intense and extend too far to the south.

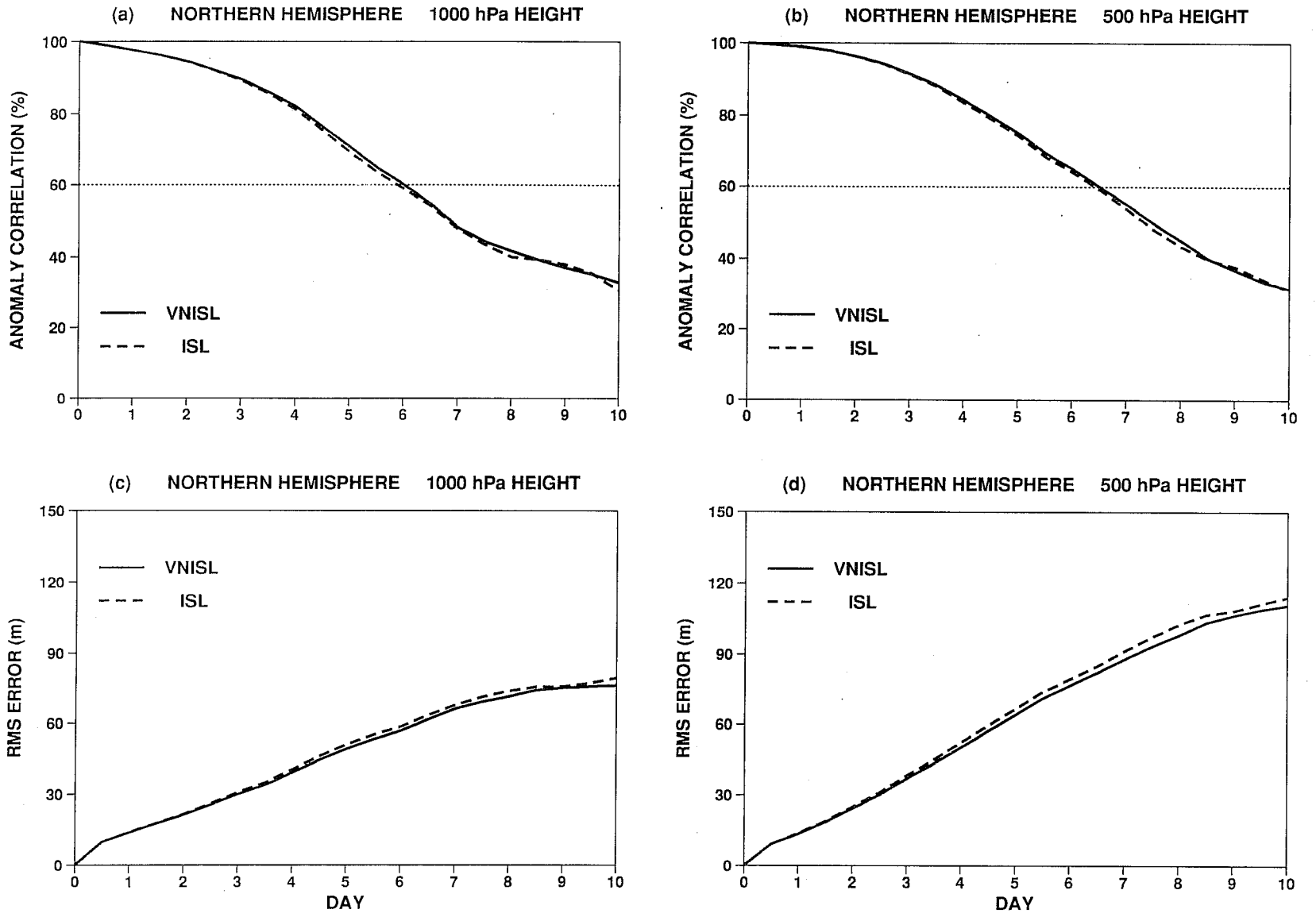

Fig. 8 Mean objective scores for the northern hemisphere comparing the vertically non-interpolating (solid) and fully interpolating (dashed) semi-Lagrangian versions:
(a) anomaly correlation of 1000 hPa height (b) anomaly correlation of 500 hPa height
(c) root-mean-square error of 1000 hPa height (metres) (d) root-mean-square error of 500 hPa height (metres).

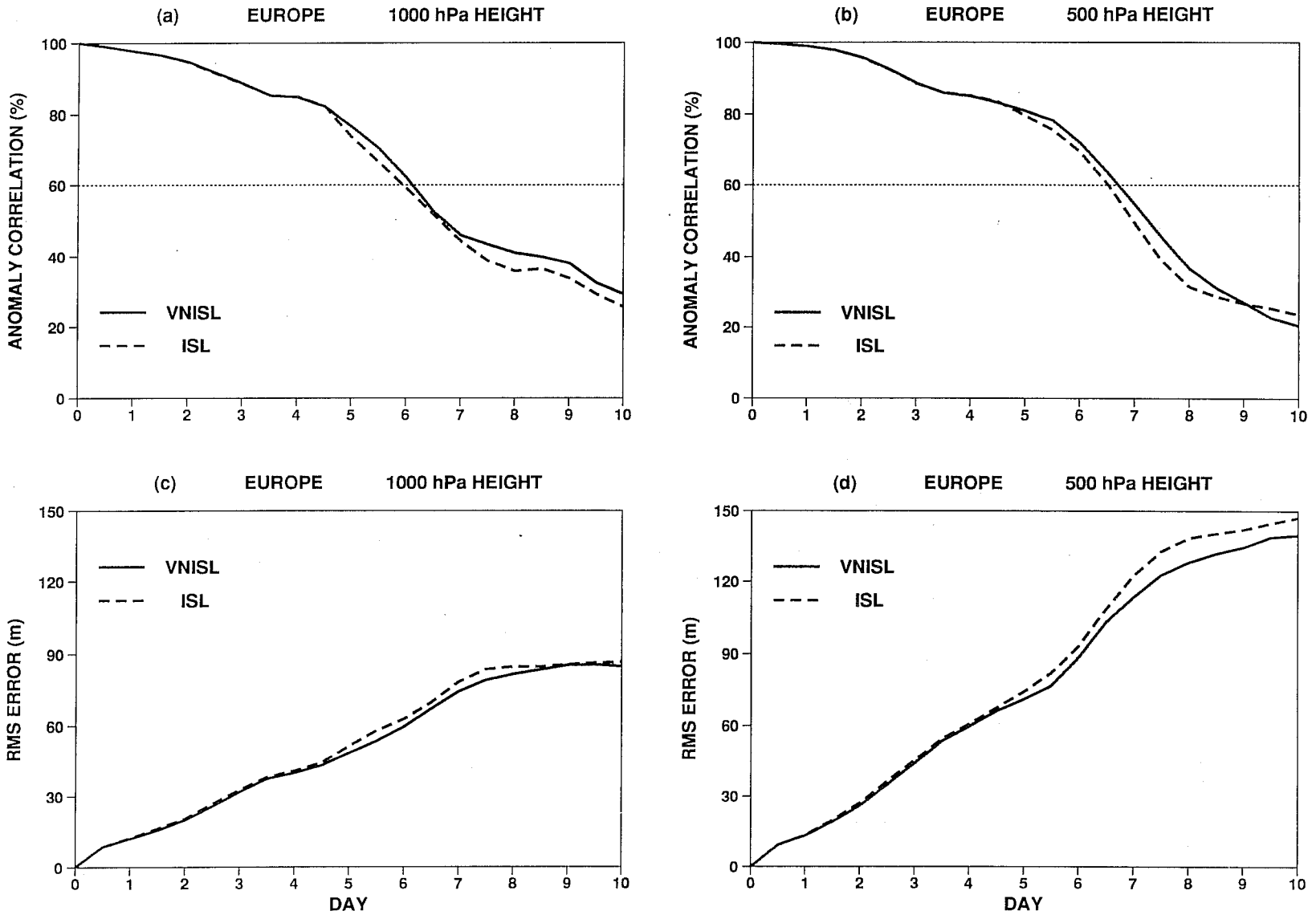

Fig. 9 As in Fig. 8 except for the European region.

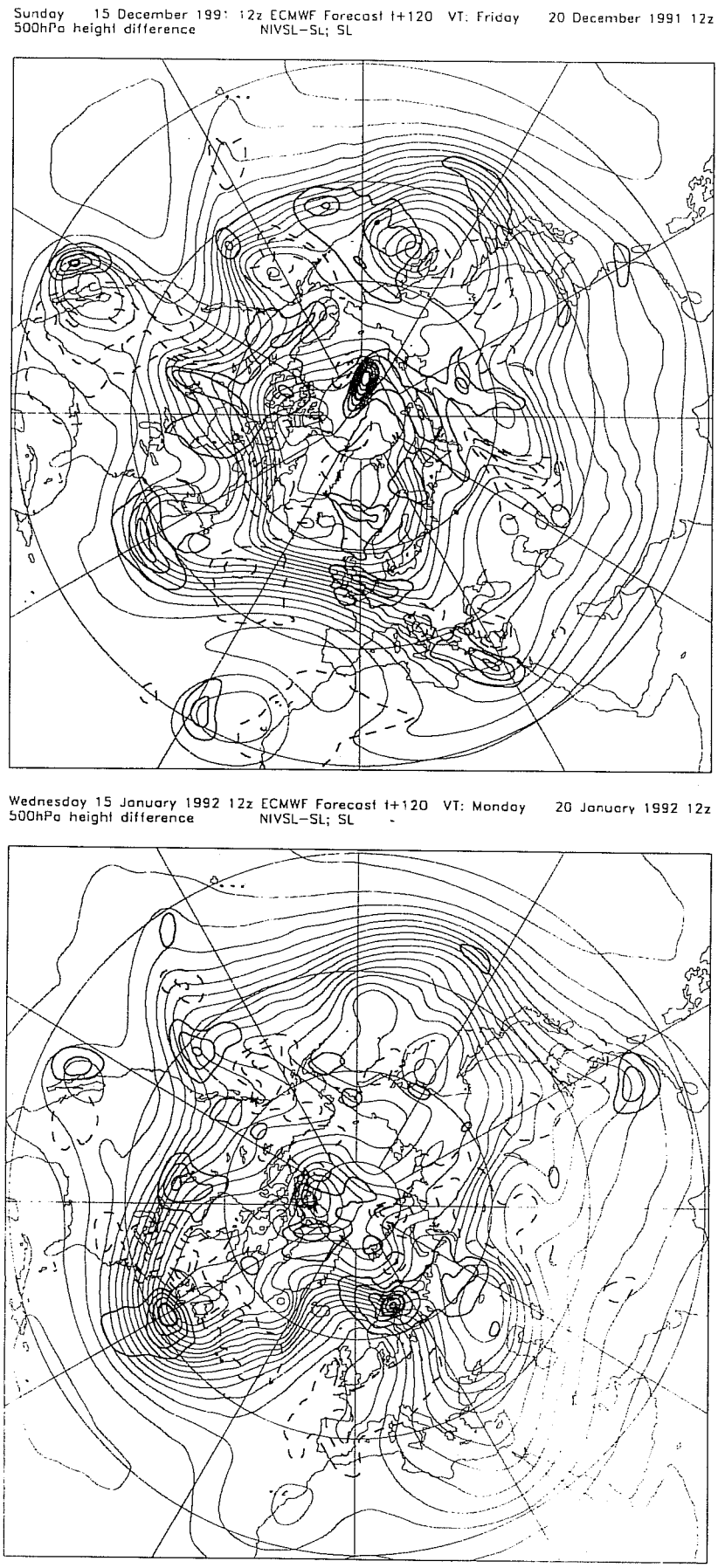

Fig. 10 Day-5 500 hPa T213/L31 height forecasts from 15 December 1991 and 15 January 1992. The fine solid lines (contour interval 6 dam) show the forecast made using the fully interpolating scheme. The heavier lines (contour interval 2 dam, negative contours dashed) show differences between the "vertically non-interpolating" and fully interpolating forecasts.

Also, differences in zonal-mean temperature between semi-Lagrangian and Eulerian forecasts are substantially reduced at upper levels when the semi-Lagrangian scheme is changed to the vertically non-interpolating form (figure not shown). The reason for the different behaviour of the fully interpolating scheme is not entirely understood. Ritchie (1991) originally attributed it to an excessive smoothing in the fully interpolating version due to vertical interpolation through the tropopause where all the dynamic fields vary abruptly in the vertical. This was based on five-day experiments with a baroclinic model that included only very simple parameterizations. More recently Williamson and Olson (1994) have examined climate simulations using a semi-Lagrangian version of the NCAR CCM2 which includes sophisticated physical parameterizations, and have concluded that the fully interpolating version actually reduces deficiencies that the former Eulerian version had in the vicinity of the tropopause. These are points that warrant further investigation. In any case, the present results in terms of medium-range forecasts with a high resolution, fully parameterized forecast model indicate a clear advantage for the vertically non-interpolating semi-Lagrangian scheme. It was implemented operationally in August 1992 and the anticipated improvement was realized. The performance of the operational T213/L31 model has subsequently been further improved by the implementation of the better radiation parameterization in February 1993, as mentioned above. This gave temperature changes around the tropopause comparable in size to those resulting from switching from the fully interpolating to the vertically non-interpolating semi-Lagrangian scheme.

Despite its advantage in terms of medium-range forecast scores, the vertically non-interpolating scheme is not superior in all respects to the fully interpolating version. In particular, it inherits from the Eulerian finite-difference vertical discretization a tendency to produce noisy and unrealistic vertical structures from time to time in synoptically quiet

regions. These unrealistic structures are not seen in the corresponding forecasts using the fully interpolating scheme. This result is consistent with the observation that semi-Lagrangian advection has better dispersive properties than finite-difference Eulerian advection (Staniforth and Côté, 1991), since as we have already noted the vertical advection is mostly handled in a purely Eulerian manner in the vertically non-interpolating scheme.

(f) Impact of increasing horizontal resolution

By virtue of its increased efficiency as presented in section 5(b), incorporation of the semi-Lagrangian scheme was very important in enabling an increase in horizontal resolution from T106 to T213 in the operational ECMWF forecast model. It is not our intention here to present an exhaustive study of the impact of horizontal resolution over a wide range of truncations. However, it is of interest to document the impact of this increase in horizontal resolution for the set of 12 cases studied here. In Figure 11 we see the marked improvement in the objective scores (mean anomaly correlations and root-mean-square height errors at 1000 and 500 hPa) for the northern hemisphere. Figure 12 presents the corresponding results for the European region. In these tests the same 31 level configuration was used for both horizontal resolutions. It is seen that this increase in horizontal resolution indeed had a very significant positive impact which, in fact, is substantially greater than the impact of any of the other changes that have been presented in the previous figures.

(g) Comments on optimizations

Several additional sets of tests were performed to study the impact of some of the optimizations that have been incorporated in the operational semi-Lagrangian T213/L31 model. These optimizations leave the objective scores virtually unchanged, but produce worthwhile extra efficiency gains that help reduce the semi-Lagrangian overheads to the 20% reported in Table 2. In particular, it was confirmed that there is no significant degradation

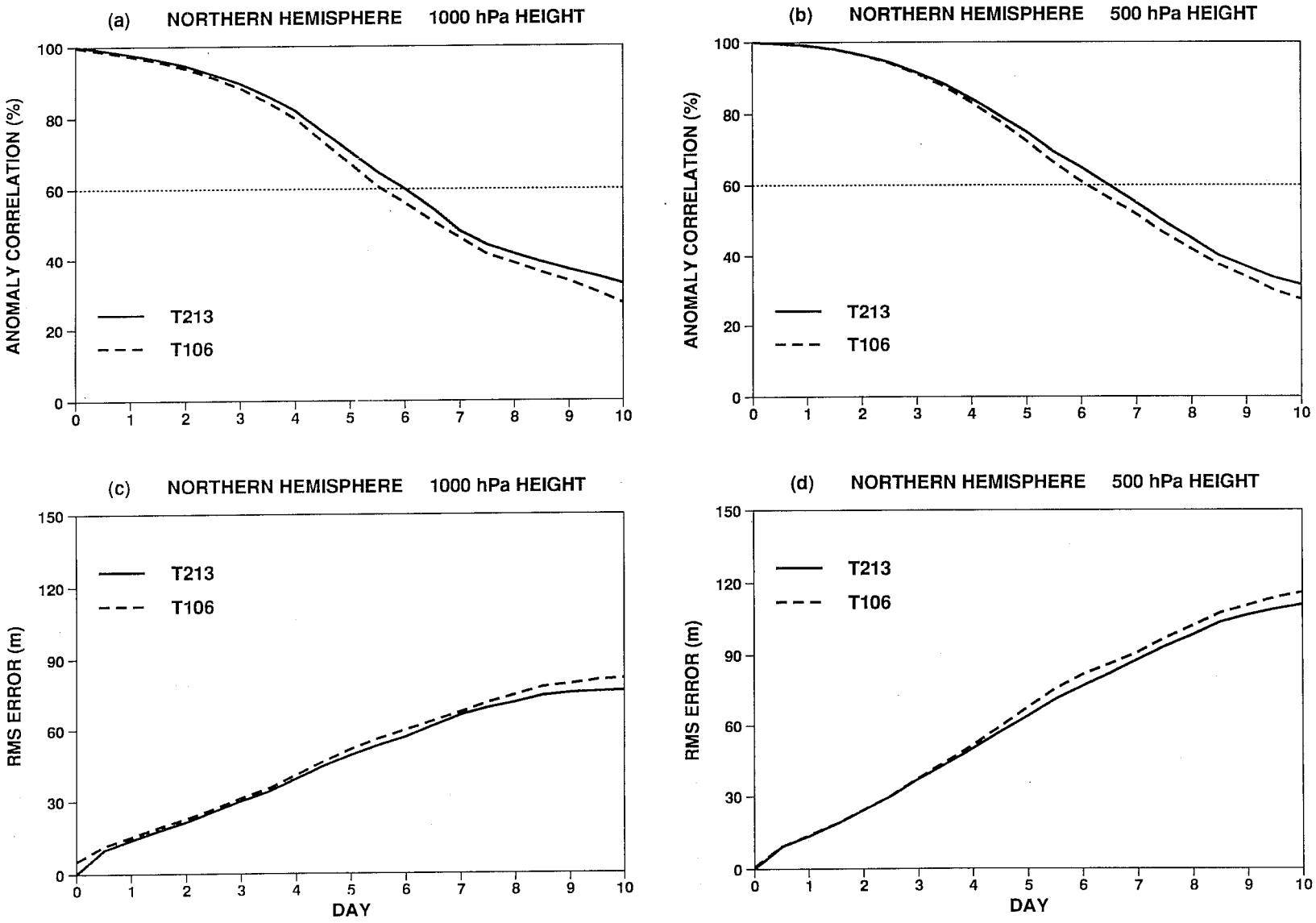

Fig. 11 Mean objective scores for the northern hemisphere comparing T213 horizontal resolution (solid) and T106 horizontal resolution (dashed):
(a) anomaly correlation of 1000 hPa height (b) anomaly correlation of 500 hPa height
(c) root-mean-square error of 1000 hPa height (metres) (d) root-mean-square error of 500 hPa height (metres).

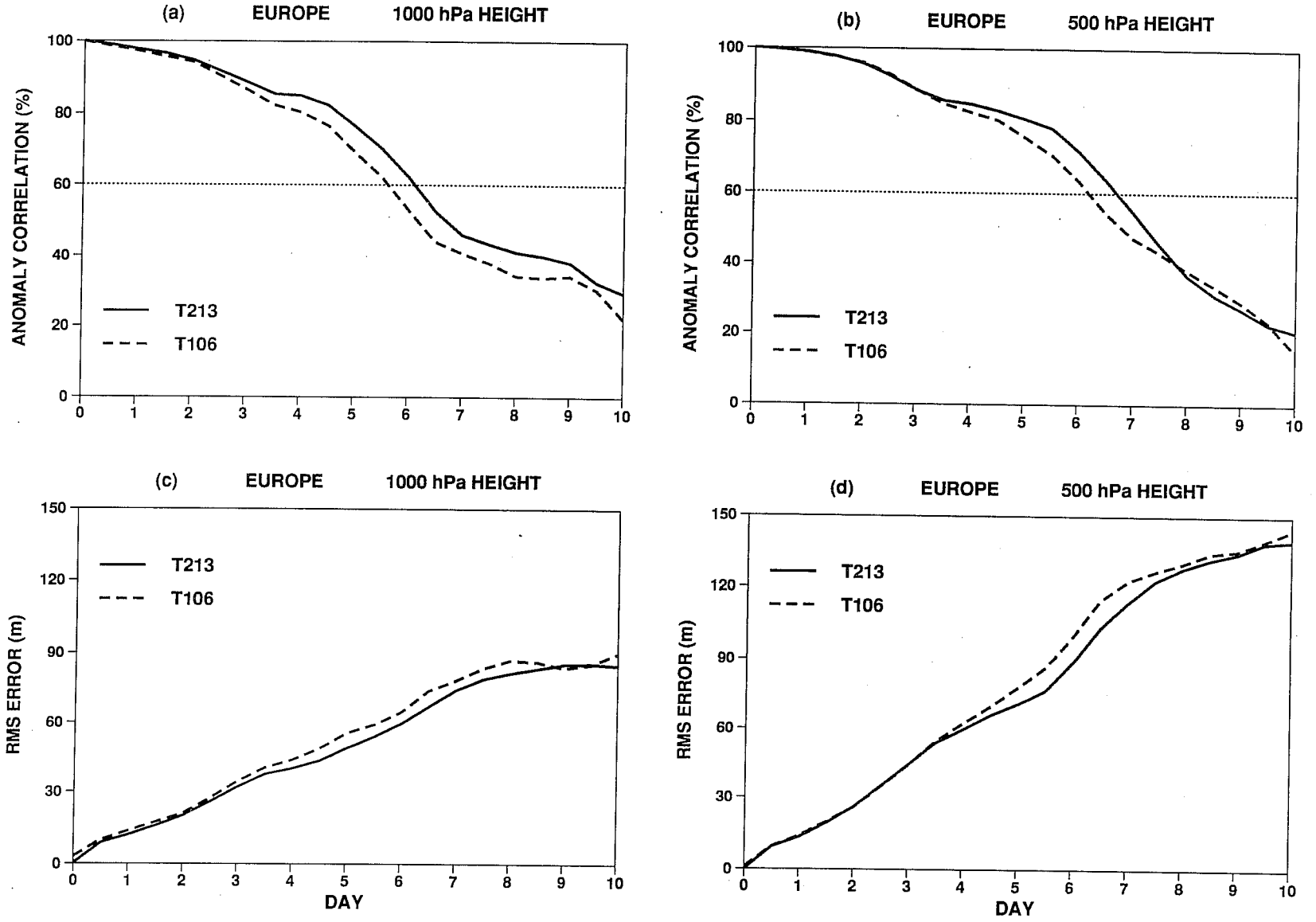

Fig. 12 As in Fig. 11 except for the European region.

resulting from using linear rather than cubic interpolation, and only one iteration rather than two, in calculating the trajectories required for the time-stepping procedure as described in section 3(f). Optimizations based on approximations to the spherical trigonometry are also used in the calculation of the departure points. The versions implemented correspond to those presented in section 2(b) of Ritchie and Beaudoin (1994), except that only the terms accurate to second order in the timestep are explicitly retained.

6. Discussion

In this article we have examined the implementation of the semi-Lagrangian method in a high resolution version of the ECMWF forecast model. In section two we presented the reformulation of the Eulerian version in order to transform the vorticity-divergence formulation into a momentum-equation version in preparation for a subsequent semi-Lagrangian vector treatment of the equation of motion. Another important aspect treated was the vertical discretization for the ECMWF hybrid coordinate on a staggered grid as designed by Simmons and Burridge for conservation of angular momentum and energy for frictionless adiabatic flow. A novel feature of the semi-Lagrangian implementation given here is its use in a baroclinic spectral model in conjunction with the reduced Gaussian grid, as described by Hortal and Simmons (1991), in which the "fully reduced grid" option leads to a savings of about 25%. The momentum equation formulation is considerably more economical than its vorticity-divergence counterpart and, by also incorporating economies in the Legendre transforms demonstrated by Temperton (1991) for the shallow-water equations, reduced the number of multi-level Legendre transforms in the reformulated Eulerian model from 17 to 12 per timestep.

The semi-Lagrangian treatment of the momentum equation formulation, including the semi-implicit correction and spatial averaging of nonlinear terms along the trajectories, was presented in section three. Linear interpolation is used for the terms evaluated at the midpoint of the trajectory, with "quasi-cubic" interpolation for the terms evaluated at the departure point. By interpolating first in the longitudinal direction, it is relatively simple to accommodate the irregular mesh resulting from the use of the reduced Gaussian grid. Adaptations required for applying the semi-Lagrangian method on the vertically staggered hybrid coordinate grid were also discussed. The number of multi-level Legendre transforms

per timestep is reduced to 10 (and potentially 8) in the semi-Lagrangian model.

Several important computational details related to this high resolution operational implementation of the semi-Lagrangian scheme were described in section 4. These include the use of memory and random access files during the three-scan structure used for advancing the forecast by one timestep, comments on the associated multitasking strategy for executing the model efficiently on a "modestly parallel" supercomputer, and some performance results. Particularly noteworthy in terms of CPU usage are that, even at this high resolution, the Legendre transforms only take about 14% of the time, and that the semi-Lagrangian calculations (which replace some transforms that would otherwise be required to calculate Eulerian advection) take about 20% of the time.

In order to assess the impact of formulation and numerical parameter changes, various experimental results on sets of 12 independent cases were presented in section 5. It was found that the semi-Lagrangian version with a 15 minute timestep gave an accuracy equivalent to that of an Eulerian version with a 3 minute timestep, giving an efficiency improvement of about a factor of 4 after allowing for the 20% of time spent in the semi-Lagrangian computations. It was noted that, with adjustments to the semi-implicit parameter (for the semi-Lagrangian version) and strength of horizontal diffusion (for the Eulerian version), both of these timesteps could be increased. Nevertheless, it remains true that the semi-Lagrangian scheme remains accurate and stable with timesteps several times longer than possible with the Eulerian scheme. It was confirmed that the hybrid-coordinate configuration of this model maintains its design advantage over the sigma-coordinate version in the stratosphere. No special filters were required in order for the application of the semi-Lagrangian method in hybrid coordinates to work successfully in this three time-level model. It was found that, even in this high resolution configuration, compared to the "fully

interpolating" version, the "vertically non-interpolating" scheme has a positive impact on the day-to-day consistency of the forecasts, the objective measures of skill, and the levels of eddy activity. On the other hand, the fully interpolating scheme produces smoother and more realistic vertical structures than either the Eulerian version or the vertically non-interpolating scheme, and it is important to understand and correct the negative aspects of its performance. Finally, it was confirmed that increasing the horizontal resolution from T106 to T213 has a significant positive impact which, in fact, is substantially greater than the impact of any of the other changes that have been presented in this implementation of the semi-Lagrangian method in the ECMWF forecast model.

To conclude the discussion, it is worth pointing out two new advantages of the spectral method which have emerged from this work. First, the combination of the spectral method with the reduced Gaussian grid provides the neatest solution yet found to the problem of defining almost-uniform resolution over the sphere. Second, the spectral method is particularly suited to semi-Lagrangian schemes: since there is no staggering of the variables in the horizontal, the difficulties of combining a semi-Lagrangian scheme with a staggered grid (expensive calculation of multiple trajectories, or loss of accuracy due to averaging) are completely avoided.

Acknowledgments. We are grateful to a number of colleagues who have contributed to the development of the high resolution version of the ECMWF forecast model. In particular we thank Dave Williamson for helpful comments during a three month visit to ECMWF when the initial testing of the T213/L31 model was in progress. The authors are also very grateful to their respective employers for their support in this mutually beneficial collaboration on the operational implementation of semi-Lagrangian semi-implicit methods in spectral models.

REFERENCES

Asselin, R., 1972: Frequency filter for time integrations. *Mon. Wea. Rev.*, **100**, 487-490.

Bates, J.R., and A. McDonald, 1982: Multiply-upstream, semi-Lagrangian advective schemes: Analysis and application to a multilevel primitive equation model. *Mon. Wea. Rev.*, **110**, 1831-1842.

Bates, J.R., S. Moorthi and R.W. Higgins, 1993: A global multilevel atmospheric model using a vector semi-Lagrangian finite-difference scheme. Part I: Adiabatic formulation. *Mon. Wea. Rev.*, **121**, 244-263.

Blondin, C., and H. Böttger, 1987: The surface and sub-surface parameterization scheme in the ECMWF forecasting system. ECMWF Research Dept. Tech. Memo. No.135, 48pp. (available from ECMWF).

Buizza, R., J. Tribbia, F. Molteni and T. Palmer, 1993: Computation of optimal unstable structures for a numerical weather prediction model. *Tellus*, **45A**, 388-407.

Côté, J., and A. Staniforth, 1988: A two-time-level semi-Lagrangian semi-implicit scheme for spectral models. *Mon. Wea. Rev.*, **116**, 2003-2012.

Côté, J., and A. Staniforth, 1990: An accurate and efficient finite-element global model of the shallow-water primitive equations. *Mon. Wea. Rev.*, **118**, 2707-2717.

Courtier, P., C. Freyder, J.-F. Geleyn, F. Rabier and M. Rochas, 1991: The ARPEGE project at Météo-France. Proceedings of the ECMWF Seminar on Numerical Methods in Atmospheric Models, 9-13 September 1991, Vol. II, 192-231 (available from ECMWF).

Courtier, P., and M. Naughton, 1994: A pole problem in the reduced Gaussian grid. *Quart. J. Roy. Meteor. Soc.*, in press.

Dent, D., 1992: Modelling and Parallelism, in "Modelling Weather and Climate", BMRC Research Report No. 33, 165-178 (available from BMRC, Melbourne, Australia).

Golding, B.W., 1992: An efficient non-hydrostatic forecast model. *Meteorol. Atmos. Phys.*, **50**, 89-103.

Hortal, M., and A.J. Simmons, 1991: Use of reduced Gaussian grids in spectral models. *Mon. Wea. Rev.*, **119**, 1057-1074.

Janssen, P.A.E.M., A.C.M. Beljaars, A.J. Simmons and P. Viterbo, 1992: The determination of the surface stress in an atmospheric model. *Mon. Wea. Rev.*, **120**, 2977-295.

Jarraud, M., A.J. Simmons and M. Kanamitsu, 1988: Sensitivity of medium range weather forecasts to the use of an envelope orography. *Quart. J. Roy. Meteor. Soc.*, **114**, 989-1025.

Leslie, L.M., and R.J. Purser, 1991: High-order numerics in an unstaggered three-dimensional time-split semi-Lagrangian forecast model. *Mon. Wea. Rev.*, **119**, 1612-1623.

Louis, J.F., 1979: A parametric model of vertical eddy fluxes in the atmosphere. *Bound.-Layer Meteor.*, **17**, 187-202.

McDonald, A., 1986: A semi-Lagrangian and semi-implicit two time level integration scheme. *Mon. Wea. Rev.*, **114**, 824-830.

McDonald, A., and J.R. Bates, 1989: Semi-Lagrangian integration of a gridpoint shallow-water model on the sphere. *Mon. Wea. Rev.*, **117**, 130-137.

McDonald, A., and J.E. Haugen, 1992: A two time-level, three-dimensional semi-Lagrangian, semi-implicit, limited-area gridpoint model of the primitive equations. *Mon. Wea. Rev.*, **120**, 2603-2621.

McDonald, A., and J.E. Haugen, 1993: A two time-level, three-dimensional semi-Lagrangian, semi-implicit, limited-area gridpoint model of the primitive equations. Part II: Extension to hybrid vertical coordinates. *Mon. Wea. Rev.*, **121**, 2077-2087.

Miller, M.J., Palmer, T.N., and Swinbank, R., 1989: Parameterization and influence of subgrid-scale orography in general circulation and numerical weather prediction models. *Meteorol. Atmos. Phys.*, **40**, 84-109.

Morcrette, J.-J., 1990: Impact of changes to the radiation transfer parameterizations plus cloud optical properties in the ECMWF model. *Mon. Wea. Rev.*, **118**, 847-873.

Purser, R.J., and L.M. Leslie, 1988: A semi-implicit semi-Lagrangian finite-difference scheme using high-order spatial differencing on a nonstaggered grid. *Mon. Wea. Rev.*, **116**, 2069-2080.

Rabier, F., and P. Courtier, 1992: Four-dimensional assimilation in the presence of baroclinic instability. *Quart. J. Roy. Meteor. Soc.*, **118**, 649-672.

Ritchie, H., 1987: Semi-Lagrangian advection on a Gaussian grid. *Mon. Wea. Rev.*, **115**, 608-619.

Ritchie, H., 1988: Application of the semi-Lagrangian method to a spectral model of the shallow water equations. *Mon. Wea. Rev.*, **116**, 1587-1598.

Ritchie, H., 1991: Application of the semi-Lagrangian method to a multilevel spectral primitive-equations model. *Quart. J. Roy. Meteor. Soc.*, **117**, 91-106.

Ritchie, H., and C. Beaudoin, 1994: Approximations and sensitivity experiments with a baroclinic semi-Lagrangian spectral model. *Mon. Wea. Rev.*, in press.

Robert, A., 1969: The integration of a spectral model of the atmosphere by the implicit method. *Proc. WMO/IUGG Symposium on NWP*, Tokyo, Japan Meteorological Agency, VII.19-24.

Robert, A., 1981: A stable numerical integration scheme for the primitive meteorological equations. *Atmos.-Ocean*, **19**, 35-46.

Robert, A., 1982: A semi-Lagrangian and semi-implicit numerical integration scheme for the primitive meteorological equations. *J. Meteor. Soc. Japan*, **60**, 319-325.

Robert, A., T.L. Yee, and H. Ritchie, 1985: A semi-Lagrangian and semi-implicit numerical integration scheme for multilevel atmospheric models. *Mon. Wea. Rev.*, **113**, 388-394.

Simmons, A.J., B.J. Hoskins, and D.M. Burridge, 1978: Stability of the semi-implicit method of time integration. *Mon. Wea. Rev.*, **106**, 405-412.

Simmons, A.J., and D.M. Burridge, 1981: An energy and angular momentum conserving vertical finite difference scheme and hybrid vertical coordinates. *Mon. Wea. Rev.*, **109**, 758-766.

Simmons, A.J., 1987: Orography and the development of the ECMWF forecast model. ECMWF Seminar on Observation, Theory and Modelling of Orographic Effects, 15-19 September 1987, Reading, U.K., Vol. 2, 129-163 (available from ECMWF).

Simmons, A.J., D.M. Burridge, M. Jarraud, C. Girard, and W. Wergen, 1989: The ECMWF medium-range prediction models: development of the numerical formulations and the impact of increased resolution. *Meteorol. Atmos. Phys.*, **40**, 28-60.

Slingo, J.M., 1987: The development and verification of a cloud prediction scheme for the ECMWF model. *Quart. J. Roy. Meteor. Soc.*, **113**, 899-927.

Smolarkiewicz, P.K., and P.J. Rasch, 1991: Monotone advection on the sphere: an Eulerian versus semi-Lagrangian approach. *J. Atmos. Sci.*, **48**, 793-810.

Staniforth, A., and C. Temperton, 1986: Semi-implicit semi-Lagrangian integration schemes for a barotropic finite-element regional model. *Mon. Wea. Rev.*, **114**, 2078-2090.

Staniforth, A., and J. Côté, 1991: Semi-Lagrangian integration schemes for atmospheric models - a review. *Mon. Wea. Rev.*, **119**, 2206-2223.

Süli, E., and A. Ware, 1991: A spectral method of characteristics for hyperbolic problems. *SIAM J. Numer. Anal.*, **28**, 423-445.

Tanguay, M., A. Simard, and A. Staniforth, 1989: A three-dimensional semi-Lagrangian scheme for the Canadian regional finite-element forecast model. *Mon. Wea. Rev.*, **117**, 1861-1871.

Tanguay, M., A. Robert, and R. Laprise, 1990: A semi-implicit semi-Lagrangian fully compressible regional forecast model. *Mon. Wea. Rev.*, **118**, 1970-1980.

Tanguay, M., E. Yakimiw, H. Ritchie, and A. Robert, 1992: Advantages of spatial averaging in semi-Lagrangian schemes. *Mon. Wea. Rev.*, **120**, 113-123.

Temperton, C., and A. Staniforth, 1987: An efficient two-time-level semi-Lagrangian semi-implicit integration scheme. *Quart. J. Roy. Meteor. Soc.*, **113**, 1025-1039.

Temperton, C., 1991: On scalar and vector transform methods for global spectral models. *Mon. Wea. Rev.*, **119**, 1303-1307.

Thépaut, J.-N., and P. Courtier, 1991: Four-dimensional variational data assimilation using the adjoint of a multilevel primitive-equation model. *Quart. J. Roy. Meteor. Soc.*, **117**, 1225-1254.

Tiedtke, M., 1989: A comprehensive mass flux scheme for cumulus parameterization in large-scale models. *Mon. Wea. Rev.*, **117**, 1779-1800.

Williamson, D.L., and J.G. Olson, 1994: Climate simulations with a semi-Lagrangian version of the NCAR CCM2. *Mon. Wea. Rev.*, in press.

Williamson, D.L., and P.J. Rasch, 1994: Water vapor transport in the NCAR CCM2. *Tellus*, **46A**, 34-51.